


Article

Characterization and Origin of Basalt-Derived Carnelian in the Mesozoic Newark Basin, New Jersey, USA

Richard A. Volkert ^{1,*},[†], Matthew L. Goring ², William H. Peck ³  and Scott D. Stanford ¹¹ New Jersey Geological and Water Survey, Trenton, NJ 08625, USA; scott.stanford@dep.nj.gov² Department of Earth and Environmental Studies, Montclair State University, Upper Montclair, NJ 07043, USA; goringm@montclair.edu³ Department of Geology, Colgate University, Hamilton, NY 13346, USA; wpeck@colgate.edu

* Correspondence: rvolkert@comcast.net

[†] This author has retired.

Abstract: Carnelian occurs locally in New Jersey in the Newark basin as medium- to coarse-size pebbles in fluvial gravel and alluvium and colluvium formed from erosion of Lower Jurassic Preakness Basalt. Vesicles and molds of glauberite are preserved on lower surfaces and botryoidal textures on the upper surfaces of some pieces. The microstructure consists of length-fast chalcedony characterized by parallel fibrous bundles overlain by repetitive, wavy extinction bands. Only peaks of α -quartz and minor moganite are recognized in X-ray diffraction patterns. Carnelian contains 97–98 wt.% SiO_2 , ~1.0 wt.% Fe_2O_3 , and 1.0–1.4 wt.% LOI; other major elements are <0.1 wt.%. Trace element abundances are low except for Y, Nb, Ta, W, Th, and U. Rare earth element (REE) patterns display heavy REE enrichment and large negative Eu anomalies. Most trace elements were mobilized from Proterozoic sources, whereas Si was likely derived from the alteration of basaltic glass in the Preakness. Carnelian $\delta^{18}\text{O}_{\text{VSMOW}}$ values are high and range from +18.3 to +31.2‰, comparable to global occurrences of volcanic rock-derived chalcedony. We propose that carnelian precipitated in the first Preakness flow from the mixing of hydrothermal fluid with meteoric water under conditions of low temperature (20–80 °C) and neutral to slightly alkaline pH.



Citation: Volkert, R.A.; Goring, M.L.; Peck, W.H.; Stanford, S.D.

Characterization and Origin of Basalt-Derived Carnelian in the Mesozoic Newark Basin, New Jersey, USA. *Minerals* **2023**, *13*, 1249. <https://doi.org/10.3390/min13101249>

Academic Editors: Iuliu Bobos and Franck Bourdelle

Received: 30 August 2023

Revised: 20 September 2023

Accepted: 22 September 2023

Published: 24 September 2023



Copyright: © 2023 by the authors. Licensee MDPI, Basel, Switzerland. This article is an open access article distributed under the terms and conditions of the Creative Commons Attribution (CC BY) license (<https://creativecommons.org/licenses/by/4.0/>).

Keywords: carnelian; moganite; Mesozoic Newark basin; Preakness Basalt; oxygen isotopes

1. Introduction

Carnelian is a variety of silica (SiO_2) that is mainly colored in some shade of red or orange. It is classified as chalcedony on the basis of its microcrystallinity and its fibrous texture (<https://www.gemdat.org>; accessed on 24 October 2022). The absence of banding in carnelian distinguishes it from agate. Because carnelian is a semiprecious gemstone that was prized by early civilizations, the focus of many studies has been mainly from an archaeological perspective, e.g., [1–3]. Some regional geological reports mention carnelians briefly [4,5]; however, studies that focus strictly on the mineralogical and geological characterization of carnelians [6,7] are scarce, especially compared to the numerous studies of other types of microcrystalline silica such as agate, opal, and chert.

A review of the archaeological and geologic literature and the mineral website Mindat (<https://www.mindat.org>; accessed on 24 October 2022) reveals that globally carnelian occurs most commonly in weakly to unmetamorphosed volcanic rocks, with a large number of occurrences in basalt of varying geologic ages. Carnelian is also present in sedimentary rocks, such as the Miocene conglomerate of the Babaguru Formation in India [4] and the Proterozoic Salmi Formation in Karelia, Russia [8], which is composed of material eroded from the underlying Deccan and Priozersk basalts, respectively, and also in stream gravels derived from erosion of these host rocks.

Carnelian in New Jersey is present only in the central part of the Mesozoic Newark rift basin (Figure 1) at a few closely spaced locations mainly along Green Brook and Stirling

Brook (Figure 2). Information is lacking on the first find of carnelian in the study area, or on the early history of its collection there, beyond a brief mention of its occurrence in mineral collecting guides from the middle 1900s [9,10]. Varieties of quartz reported from the Newark basin in New Jersey include amethyst, smoky quartz, clear quartz crystals, pale-colored chalcedony, and agate in the Jurassic basalt formations [11], and amethyst, milky quartz, clear quartz crystals, pale-colored chalcedony, and opal in Jurassic diabase and references therein [12]. No reference is made to carnelian or other synonymous names such as cornelian, red chalcedony, or sard in any of the New Jersey mineral inventories [13–15] or studies on the occurrence and diversity of zeolites and associated secondary minerals in basalt and diabase in the Newark basin [11,12,16–21].

We are unaware of any prior scientific inquiries undertaken to study carnelians in New Jersey, and this paper presents the results of the first detailed study of samples collected from locations at Green Brook and Stirling Brook (Figure 2). This study was designed to characterize carnelian in the context of the field relationships of host bedrock and surficial lithologies, in combination with results from optical petrographic microscopy, X-ray diffraction (XRD) analysis, major and trace element geochemistry, and oxygen isotope analysis. Collectively, these data provide important constraints on the provenance of the carnelian, as well as the characteristics and source of the mineralizing fluid from which it precipitated. Although carnelian has not been recognized in situ in bedrock in the study area, the results of this study provide adequate information from which reasonable interpretations regarding its origin may be made. We refer to the samples of this study as carnelian because of their predominant red color, although we recognize they could also correctly be termed a red-colored variety of chalcedony.

2. Geologic Setting

The Mesozoic Newark basin in northern and central New Jersey is a northeast-trending half-graben formed during Triassic and Jurassic rifting of the eastern North American margin. It is in fault contact on the west with Mesoproterozoic rocks of the New Jersey Highlands and is unconformably overlain on the east by Cretaceous sediments of the Atlantic Coastal Plain (Figure 1). The Newark basin contains a succession of west-dipping, interbedded terrestrial sedimentary formations, and mafic igneous rocks. These include Upper Triassic to Lower Jurassic conglomerate, sandstone, siltstone, and shale of fluvial and lacustrine origin, three Lower Jurassic continental flood basalt formations (Orange Mountain Basalt, Preakness Basalt, and Hook Mountain Basalt), and several Lower Jurassic diabase bodies, the largest of which is the Palisades sill (Figure 1).

Bedrock formations in the area of the carnelian locations include the sedimentary Feltville Formation and the overlying Preakness Basalt (Figure 2). The 145 m thick Feltville Formation consists of reddish-brown or light-grayish-red, fine- to coarse-grained sandstone, siltstone, and silty shale composed of varied amounts of quartz, white mica, and feldspar that was deposited in a fluvial environment [22,23]. Near the base of the Feltville are two 3 m thick sequences of dark gray to black, carbonaceous shale, light-gray limestone, calcareous siltstone, and gray or olive shale deposited in a shallow- to deep-water lacustrine setting [22–24]. About 0.5 m of the uppermost beds of the formation are thermally altered along the contact with the Preakness Basalt.

The 315 m thick Preakness Basalt has a geochemical composition that corresponds to high-iron, quartz-normative tholeiitic basalt (Table 1). It consists of at least three flows of subaerially erupted dark greenish-gray to black, generally fine-grained basalt that yield a zircon U-Pb crystallization age of 201 ± 0.03 Ma [25]. It contains (modal%) 45%–51% andesine or labradorite, 38%–44% augite, 4%–6% Fe-Ti oxides, and 3%–6% mesostasis composed of fine-grained intergrown plagioclase, K-feldspar, Fe-Ti oxides, apatite, quartz, and altered clinopyroxene [26]. Zeolites are rare in the Preakness compared to their abundance in the stratigraphically overlying Hook Mountain Basalt and the underlying Orange Mountain Basalt. The base of the 125 to 145 m thick Preakness first flow contains vertical, slender, and prismatic columnar joints up to 0.5 m wide and 6 m long [27] that rest

on the contact with the Feltville Formation. At several locations, including the study area, the base of the first flow is pillowed and vesicular [22,28,29], indicating a local subaqueous eruption. Where present, pillows are as much as 0.6–0.9 m in diameter and occur over a 3- to 10- m- thick interval [28,29]. They are in contact with an intercalated layer of gray or brown basaltic glass as much as 2.5 cm thick [30]. The pillowed intervals are overlain by slender columnar jointed basalt that elsewhere defines the base of the first flow.

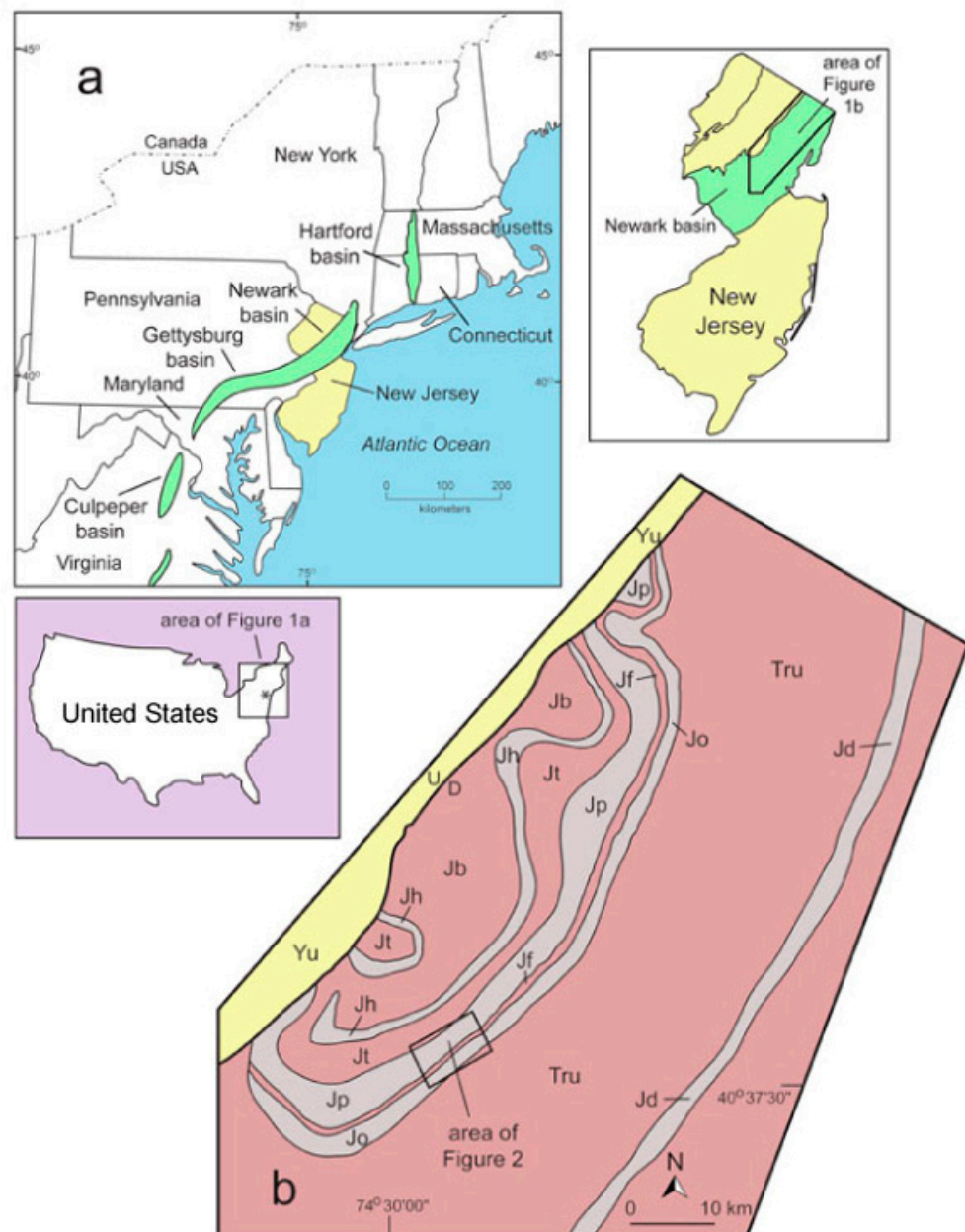


Figure 1. (a) Distribution of Mesozoic-age rift basins (green) in eastern North America. Small inset maps locate New Jersey (asterisk) in the United States and the Newark basin in northern New Jersey. (b) Simplified bedrock geologic map of igneous (gray) and sedimentary formations (red) in the northern and central parts of the Newark basin modified from [31]. Symbols: Jd, Palisades diabase; Tru, undivided Triassic sedimentary formations; Jo, Orange Mountain Basalt; Jf, Feltville Formation; Jp, Preakness Basalt; Jt, Towaco Formation; Jh, Hook Mountain Basalt; Jb, Boonton Formation; Yu, undivided Mesoproterozoic rocks. U and D show normal movement sense on the Mesozoic border fault separating Mesoproterozoic rocks and Mesozoic rocks in the Newark basin.

Coarse-grained gabbroid (Figure 3a) forms concordant layers that are as much as 80 m thick within the middle and upper parts of the first flow (Figure 2). Gabbroid layers have sharp upper contacts and gradational lower contacts with the host basalt from which it was formed through fractionation [26]. The geochemical composition of gabbroid and intercalated glass-rich gabbroid is given in Table 1. The mineralogy of gabbroid is comparable to that of fine-grained host basalt except for the coarse grain size in which clinopyroxene and plagioclase attain lengths of up to 2 cm. Gabbroid layers 12–36 m beneath the top of the first flow contain dark red or black vitreous glass (Figure 3b). The uppermost part of the first flow consists of blocky and massive basalt overlain at the top by a highly vesicular and amygdaloidal layer ~2.5 m thick (Figure 3c).

Table 1. Geochemical composition of lithologies in the Preakness Basalt.

| | Basalt; First Flow Base (n = 4) | Basalt; 20–75 m above Base (n = 17) | Gabbroid; 85–130 m above Base (n = 5) | Glass-Rich Gabbroid (n = 2) | Vesicular Gabbroid 140 m above Base (n = 2) | Basalt; 25 m above Gabbroid (n = 2) | Basalt; Top of First Flow (n = 2) | Basalt; Second Flow Base (n = 1) |
|---|--|--|--|-----------------------------------|---|--|--|--|
| SiO ₂ | 51.59 | 52.43 | 53.35 | 53.48 | 53.93 | 52.72 | 50.30 | 52.75 |
| TiO ₂ | 1.05 | 0.91 | 1.38 | 1.15 | 1.74 | 1.05 | 1.06 | 1.09 |
| Al ₂ O ₃ | 14.35 | 14.42 | 12.18 | 10.62 | 10.58 | 13.91 | 12.97 | 13.95 |
| Fe ₂ O ₃ ^t | 13.19 | 11.81 | 14.63 | 15.34 | 16.66 | 13.59 | 13.65 | 13.19 |
| MnO | 0.21 | 0.20 | 0.22 | 0.23 | 0.25 | 0.21 | 0.24 | 0.22 |
| MgO | 5.54 | 6.33 | 4.75 | 3.41 | 3.92 | 5.48 | 8.01 | 6.04 |
| CaO | 10.90 | 9.50 | 7.05 | 7.88 | 5.72 | 8.52 | 6.79 | 10.05 |
| Na ₂ O | 2.98 | 3.03 | 3.69 | 4.51 | 2.77 | 3.54 | 3.97 | 2.49 |
| K ₂ O | 0.62 | 0.69 | 0.46 | 0.06 | 1.10 | 0.79 | 0.37 | 0.62 |
| P ₂ O ₅ | 0.14 | 0.17 | 0.20 | 0.63 | 0.33 | 0.13 | 0.18 | 0.14 |
| LOI | 0.72 | 0.89 | 1.77 | 2.33 | 2.46 | 0.85 | 2.29 | n.d. |
| Rb | 18 | 24 | 28 | n.d. | n.d. | 25 | n.d. | 20 |
| Sr | 151 | 143 | 114 | 69 | 108 | 152 | 137 | 132 |
| Y | 27 | 27 | 40 | n.d. | n.d. | 27 | 27 | 26 |
| Zr | 87 | 83 | 122 | 207 | 168 | 87 | 93 | 86 |
| Nb | 4.5 | 3.8 | 7.1 | n.d. | n.d. | 4.3 | 3.9 | 4.7 |
| Hf | 2.3 | 2.1 | 3.8 | n.d. | n.d. | 2.3 | 2.1 | 2.4 |
| Ta | 0.30 | 0.34 | 0.58 | n.d. | n.d. | 0.34 | 0.33 | 0.40 |
| Pb | 6.0 | 6.0 | 5.3 | n.d. | n.d. | 4.0 | 7.0 | 6.0 |
| Th | 2.0 | 2.0 | 4.0 | n.d. | n.d. | 2.0 | 2.0 | 2.0 |

Major elements in wt.%; trace elements in ppm; Fe₂O₃^t, total iron as Fe₂O₃; LOI, loss on ignition; n, number of samples; n.d., not determined. Data sources: [26,32].

The first and second Preakness flows are separated by ~2–3 m of thin-bedded, reddish-brown, fluvial siltstone and shale (Jps1) deposited on the top of the first flow (Figures 2 and 3c). The base of the 70 m thick second flow typically consists of massive basalt containing pipe vesicles overlain by widely spaced, blocky, columnar joints. The rest of the second flow is composed of relatively massive basalt intercalated with a few very thin gabbroid layers.

3. Methods

Three samples of carnelian from Green Brook, two red and one reddish-orange, and two samples from Stirling Brook, one reddish-orange and one yellow, were analyzed at Montclair State University on a Philips X'Pert MPD X-ray diffractometer. Samples were wet ground in a porcelain mortar in acetone and powdered to ≤200 mesh. They were analyzed using CuK α radiation, with runs between 5° and 75° 2 θ at 45 kV and 40 mA at a step size of 0.02° and a scan rate of 1.2°/min. The crystallite size of the 101 quartz peak was calculated using the Scherrer equation $K\lambda/(\beta\cos\theta)$, in which K is a dimensionless shape factor = 0.94, λ is the wavelength in Å of CuK α = 1.5418, β is the full width at half maximum (FWHM) °2 θ , and θ is $\frac{1}{2}$ of the 101 peak position °2 θ . The lattice microstrain was calculated using the equation $\beta/4\tan\theta$, in which β is the FWHM °2 θ and θ is the 101 peak position in °2 θ .

Because of insufficient sample material from Stirling Brook, three samples of red carnelian from Green Brook were analyzed for major, trace element, and REE abundances at Activation Laboratories in Ontario, Canada. The samples were pulverized to 95% 200 mesh in a mild steel mill. Powders underwent lithium metaborate/tetraborate fusion followed by rapid digestion in a weak nitric acid solution. Whole-rock analysis of major elements, Sc, V, Sr, and Ba, was determined by inductively coupled plasma (ICP) optical emission spectrometry. All other trace elements and REE were analyzed by ICP mass spectrometry. Loss on ignition was determined by gravimetric analysis.

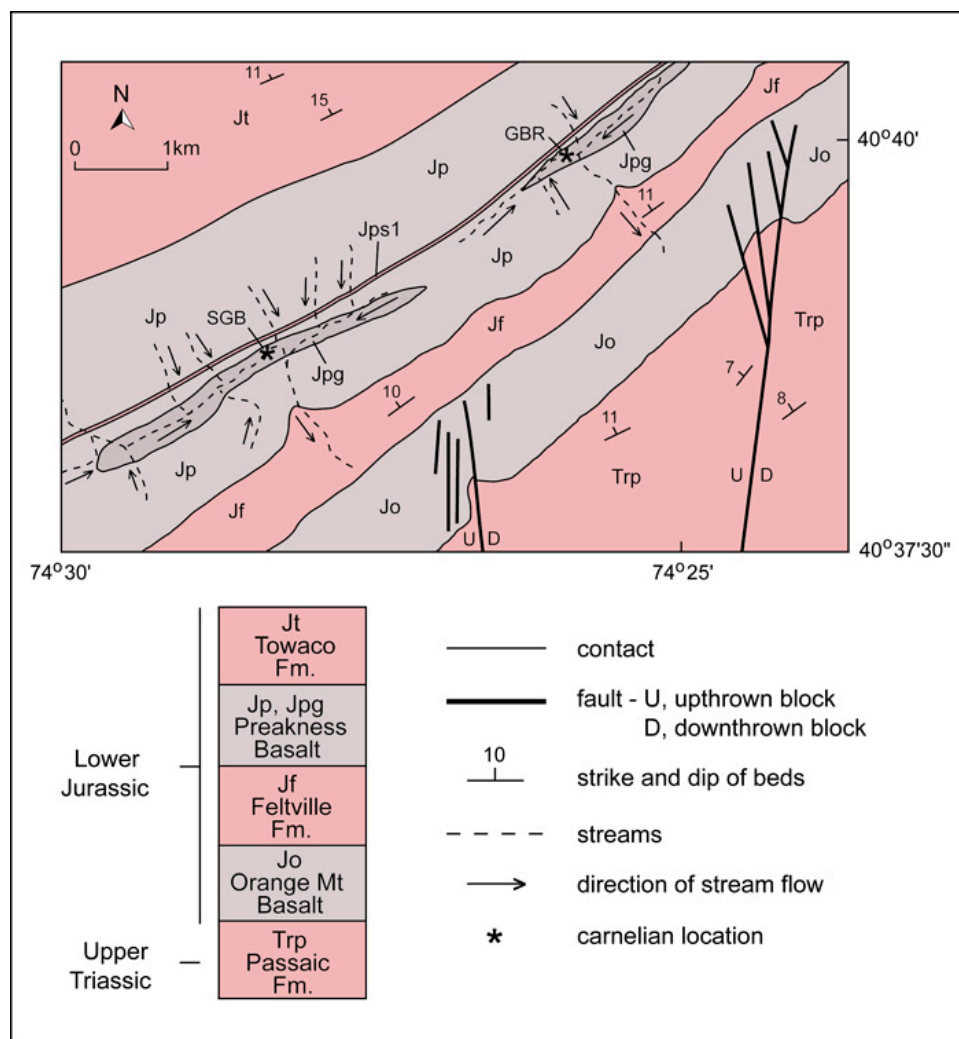


Figure 2. Bedrock geologic relationships in the study area modified from [33]. Carnelian sample locations (shown as asterisks) are labeled GBR (Green Brook) and SGB (Stirling Brook) and are keyed to samples in Tables 2–4. Jpg, gabbroid bodies; Jps1, the sedimentary layer deposited on top of the first Preakness flow. Other symbols as in Figure 1.

Six samples of carnelian from Green Brook, three red, one reddish-orange, and two yellow, were analyzed for oxygen isotope ratios at the Stable Isotope Laboratory at Northern Illinois University. Carnelian separates weighing 1.0–1.5 mg were heated with a Photon Machines Fusions 10.6 μm CO_2 laser in the presence of 10 kPa of BrF_5 to generate O_2 gas [34]. Oxygen was transferred cryogenically by adsorption on a zeolite trap to a Thermo MAT253 isotope ratio mass spectrometer for analysis. $\delta^{18}\text{O}$ is reported in conventional per mil values relative to Vienna Standard Mean Ocean Water (VSMOW) and calibrated to IAEA quartz standard NBS-28 ($\delta^{18}\text{O} = 9.6\text{‰}$) and an internal quartz standard ($\delta^{18}\text{O} = 18.2\text{‰}$).

Five out of the six samples analyzed were duplicated or triplicated. On the day of analysis, NBS-28 had an average precision (1σ) of $\pm 0.11\%$ ($n = 4$), and the internal standard had an average precision of $\pm 0.10\%$ ($n = 3$).

4. Carnelian

4.1. Field Relationships

Carnelian in the study area is recognized from only a few closely spaced locations that are underlain by the Preakness Basalt, and more specifically by coarse-grained gabbroid in the upper part of the first flow (Figure 2). Gabbroid is intermittently exposed at these locations as small outcrops along stream banks or pavement outcrops in stream beds (Figure 3d). Gabbroid attains a calculated thickness of about 82 m at Green Brook and 49 m at Stirling Brook, the former being one of the thickest bodies recorded in the Preakness in the Newark basin. The trend of the carnelian locations falls along a prominent northeast-striking valley that is bordered by ridges to the northwest and southeast. These ridges are underlain by the Preakness and are concordant to the strike of outcropping bedrock formations (Figure 2). The western ridge is underlain by the second flow and the eastern ridge by the first flow and intercalated gabbroid layers. The western part of the valley between the ridge crests marks the eroded top of the first flow that was subaerially exposed at 201 Ma long enough for ~2 m of sediment to have been deposited on the vesicular flow top (Figure 3c) prior to the eruption of the second flow.

Much of the bedrock in the study area is covered by a veneer of weathered basalt and colluvium as much as 18 m thick composed of angular to subangular basalt pebbles and cobbles with a clayey silt to clayey sand matrix [35]. On gentle footslopes and floodplains, colluvium and weathered basalt are overlain by up to 3 m of alluvium composed of silty sand to clayey silt [35]. Carnelian is found principally in fluvial gravel bars deposited on gabbroid in Green Brook (Figure 3d) and Stirling Brook. Gravel bars at the carnelian locations are composed entirely of Preakness Basalt and gabbroid (Figure 3e). Absent in the gravel is reddish-brown sediment eroded from the Feltville Formation or the thin layer of sediment that separates the first and second Preakness flows. At Stirling Brook, carnelian is also present in fine-grained alluvium and slope wash deposited on a gentle terrace adjacent to the stream (Figure 3f).

It is particularly noteworthy that the carnelian locations are present south of the Wisconsin terminal moraine and occur outside the basins of glacial lakes. The Stirling Brook location (SGB in Figure 2) is south of the limit of an early Pleistocene glaciation, and no glacial erratics have been observed in its drainage basin. The headwaters of the northeastern tributary of Green Brook (northeast of GBR in Figure 2) are within the early Pleistocene glacial limit because there is an occurrence of till of this glaciation there [35]. However, carnelian has not been observed nor reported in this till. The southwestern tributary of Green Brook (on which GBR is located in Figure 2) drains from unglaciated terrain, and no erratic material occurs in its basin. These observations indicate that carnelian was derived from a local source and that it was not glacially eroded and transported from Mesozoic or older bedrock lithologies that crop out to the north or west.

4.2. Provenance of New Jersey Carnelian

Because carnelian has not been observed in situ in bedrock outcrops in the study area, it was necessary to evaluate a number of potential sources. Parts of the Newark basin in New Jersey were inhabited historically by Lenni Lenape Indigenous peoples, so we first considered that carnelian may have been imported to the study area through trade from outside of the region. This seems unlikely for several reasons. If carnelian was introduced as a product of trade, then it should be found over a more widespread area and not confined to the very small area of this study. Furthermore, none of the pieces of carnelian collected show evidence of having been worked, suggesting that smaller pieces are naturally sized and shaped and do not represent debitage. The archaeological literature for New Jersey mentions chert, flint, and jasper but does not indicate that carnelian or red chalcedony

were worked as lithic material by the Lenape [36]. We thus conclude that carnelian was not imported from outside of the study area.

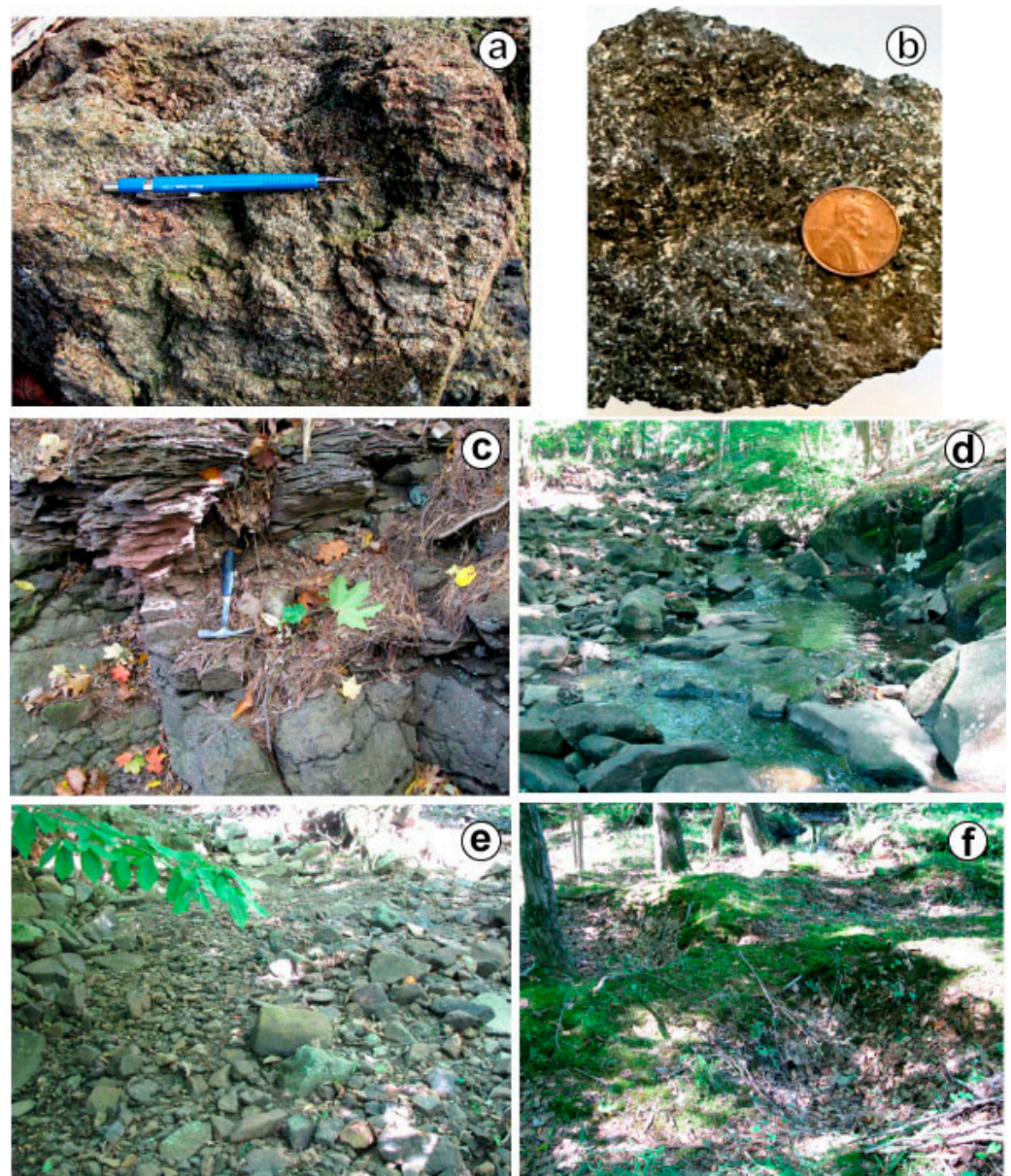


Figure 3. (a) Outcrop photograph of Preakness gabbroid from the study area representative of bedrock beneath the carnelian locations. The pencil is 14 cm. (b) Hand sample of glass-rich gabbroid from the study area. The coin is 19 mm. (c) Vesicular and amygdaloidal top of the Preakness first flow overlain above hammer by reddish-brown shale and shaly siltstone. (d) Preakness gabbroid along Green Brook in stream bank and stream bed. Angular to subangular gabbroid boulders in the channel were eroded from nearby outcrops. Small gravel bars are deposited on pavement outcrops of gabbroid in stream beds and between the boulders. (e) Fluvial gravel bar along Green Brook composed of mainly cobble- to coarse-gravel-size alluvium of Preakness Basalt and gabbroid. Finer gravel has been winnowed out and transported downstream during times of stream flooding. (f) Pits dug by collectors into alluvium and colluvium deposited near the base of the slope along Stirling Brook (visible in the top center of the photo). Carnelian is also found in gravel bars in the stream bed.

Carnelian may have formed as a silica-rich layer or part of a clast population within a sedimentary formation in, or near, the study area. However, the available evidence does not support a sedimentary provenance on the basis of the following. Carnelian has not been

recognized in nodules or siliceous layers in sedimentary formations of the Newark basin, either in outcrop or in drill-core samples that have penetrated their entire thickness [24,31]. More specifically, it is not recognized in sedimentary formations in the study area [33]. Therefore, the silicification of carbonate-rich beds or the complete replacement of carbonate nodules by silica in a manner described by [37] is not supported by geologic relationships. Furthermore, carnelian or red chalcedony is not a lithologic component of clasts in any of the conglomerates or pebbly sandstones in the Newark basin. Finally, eroded remnants of sedimentary rock that occur stratigraphically above, beneath, or within the Preakness Basalt are absent in the stream gravels in which carnelian is found.

The Orange Mountain Basalt (Figure 2) contains abundant zeolite and secondary silica mineralization in vesicles, vugs, and interstices between pillows. The first flow has undergone locally extensive hydrothermal alteration [38], and glauberite casts are recognized in pillowed intervals in the upper part of the basalt [11,19,21,22]. It is tempting to invoke the Orange Mountain as the source of carnelian, but there are fundamental problems in doing so. Carnelian is not recognized in Orange Mountain Basalt despite excellent exposure of the entire thickness of the basalt formation in a quarry <2 km southeast of the study area. Additionally, the development of the deep valley between Orange Mountain and Preakness Basalt that is underlain by the Feltville Formation preceded the formation of the valleys in which carnelian is present because they are drained by headwater tributaries of the streams in the intermontaine valleys (Figure 2). This would have prevented any river flow or material eroded from Orange Mountain and Feltville from entering the valleys of the study area. This is evidenced by the fact that the basalt colluvium mixed with carnelian is representative of the Preakness but not Orange Mountain or Feltville Formation.

We conclude that Preakness Basalt is the source of the carnelian based on the available evidence. Streams in the valley in which carnelian is found have historically received bedrock eroded from outcrops of the Preakness first and second flows (Figure 2). The location of carnelian occurrences in fluvial gravel deposited on pavement outcrops of Preakness gabbroid and also at the foot of hillslopes underlain by the Preakness in unglaciated terrain strongly suggest that carnelian originated from this basalt formation. Neogene fluvial gravels, containing rounded pebbles of quartz, quartzite, and chert, in upland settings in central New Jersey south of the study area (and south of the Lower Jurassic basalt formations), indicate that a regional river drained southward across northeastern New Jersey in the middle to late Miocene [39]. This river plain was at, or above, the elevation of the highest summits of the basalt ridges and >50 m above the elevation of the carnelian locations. Any gravel carried by this river would have been completely eroded during the formation of the modern valleys during the Pliocene and Pleistocene, and no Neogene fluvial gravel clasts have been observed in the upland areas of the basalt formations. Furthermore, the absence of significant abrasion and rounding of the carnelian pieces, in combination with the preservation of features such as botryoidal textures and glauberite molds, do not support the long-distance fluvial transport of carnelian and are more compatible with its derivation from a local source.

Two different scenarios are advanced to explain the apparent absence of carnelian in Preakness Basalt or gabbroid outcrops at the present erosion level. (1) Over time, carnelian was largely removed from the bedrock source through erosion, and what remains is preserved in gravel bars and fluvial sediments; or (2) carnelian continues to be eroded from the bedrock source that is now covered in stream beds by a veneer of alluvium and is replenished periodically during times of erosive stream flooding. The second scenario seems more likely given that carnelian continues to be found despite decades of robust collecting.

4.3. Physical Characteristics

Samples of carnelian are massive and compact, translucent, have a waxy luster, and are microcrystalline. They are mainly colored red (Figure 4a) and much less commonly reddish-orange or yellow. Banding is absent in all pieces collected, and none contain

macroscopic quartz crystals. Carnelian pieces are subangular to subrounded (Figure 4a), and they vary in diameter from 1.0 to 5.5 cm, corresponding to a medium to very coarse pebble gravel. Various features are recognized in the carnelian samples, but these are not present in all pieces. A vesicular texture that is convex upward into the carnelian (Figure 4b) appears to be an attachment surface to the bedrock, suggesting that it likely precipitated over an amygdaloidal layer. Some pieces display a botryoidal texture (Figure 4c) presumed to have formed on upper surfaces. Molds of dissolved glauberite crystals as much as 4 mm wide and 1.5 cm long (Figure 4d) around which the carnelian formed are preserved on some surfaces. The identification of glauberite was made through comparison with images of similar glauberite crystals from the Newark basin featured in previous publications [11,40].

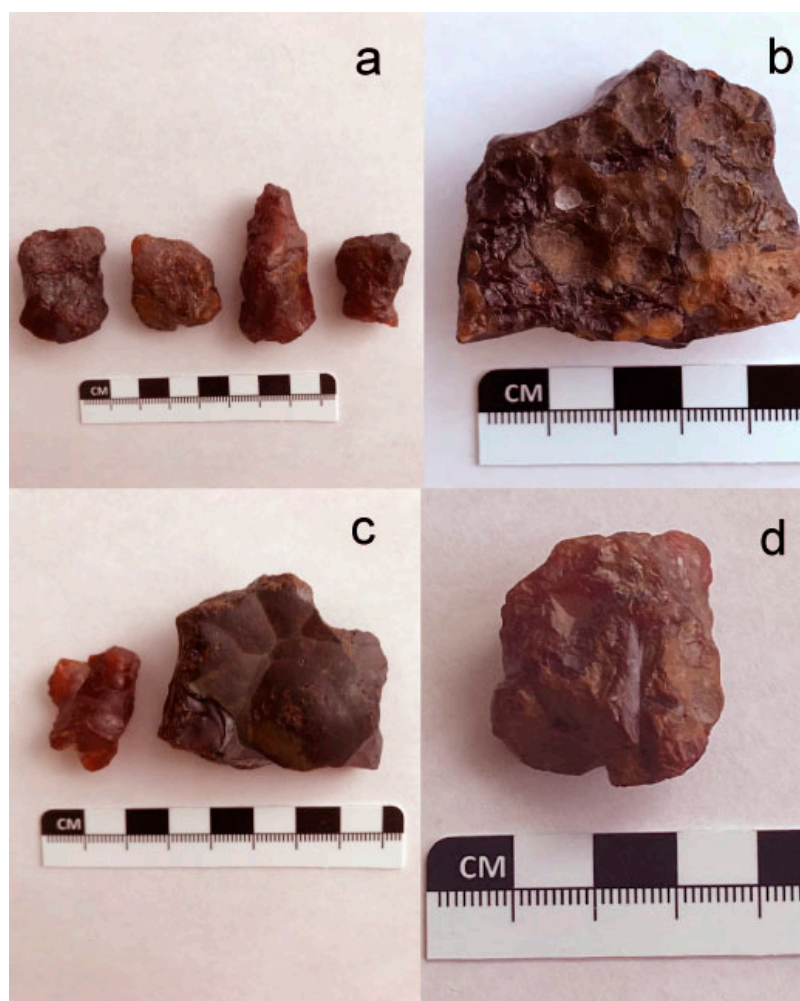


Figure 4. Representative features preserved on surfaces of carnelian from Green Brook. (a) Characteristic pieces of reddish-brown to red, subangular to subrounded, pebble gravel. (b) The lower surface displays a spheroidal, convex-upward texture presumed to have formed along an attachment surface on amygdaloidal basalt. (c) Botryoidal texture preserved on upper surfaces. (d) Lower surface displaying molds of glauberite.

4.4. Optical Petrographic Microscopy and X-ray Diffractometry

A representative sample of red carnelian from Green Brook was examined by optical petrographic microscopy, and the micrographs are presented in Figure 5. The sample is composed of microcrystalline quartz in which individual parallel fibrous bundles nucleate from an attachment surface and display elongated growth that intersects adjacent bundles (Figure 5a). These fiber bundles are optically length fast. They are in contact along the direction of elongation with repetitive extinction bands that have a zig-zag appearance due

to twisting around the fiber axis (Figure 5b). The thickness, or twist period, remains fairly uniform along the entire fiber length.

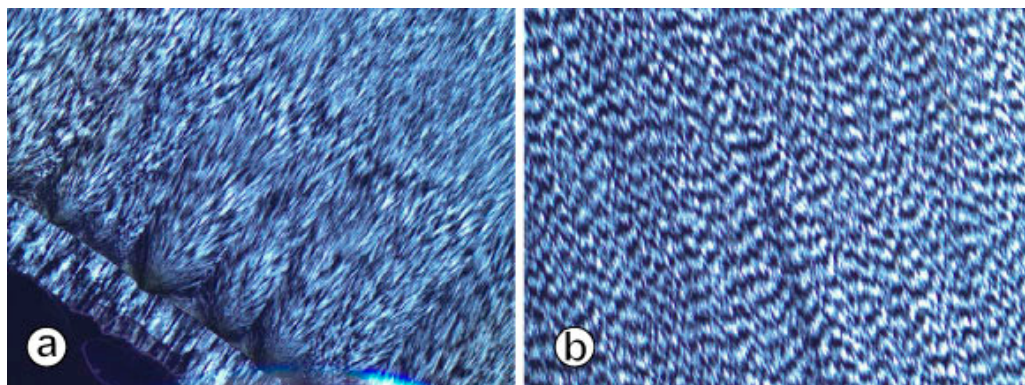


Figure 5. Optical photomicrographs in cross-polarized light showing the microstructure of carnelian from Green Brook (sample GBR 1). (a) Length-fast parallel fibrous bundles nucleating from a thin band of microcrystalline quartz presumed to be an attachment surface to basalt. The fiber elongation direction is toward the upper right. (b) Parallel aggregates of twisted fibers showing rhythmic extinction bands (wrinkle bands). The direction of elongation is toward the bottom. The horizontal field of view is 2 mm in both photomicrographs.

XRD patterns of all carnelian sampled from the Green Brook and Stirling Brook locations are similar and are dominated by major peaks of α -quartz at 3.34–3.32 Å, 4.25–4.23 Å, and 1.81 Å (Figure 6). Also observed are minor peaks at 4.45 Å, 4.38 Å, 3.09 Å, and 2.88 Å that correspond to the length-slow silica polymorph moganite [41,42]. Between about 20° and 60°, 2θ all of the XRD patterns display additional small peaks that also correspond to moganite (Figure 6). Especially significant is the fact that none of the forms of opal (C, CT, or A), cristobalite, or calcite were identified in the XRD patterns.

Quantification of the moganite content in the carnelian sampled was not performed but must be at least 5% because at contents less than that moganite peaks are unable to be resolved from quartz peaks [43]. The recognition of moganite in association with the sampled carnelian is noteworthy because to the best of our knowledge moganite has not been reported previously in New Jersey. However, a carnelian/moganite association is not unique and has been identified in carnelian analyzed from Libya that contains between 3 and 20% moganite [6]. Moganite is also reported as a common component in global occurrences of agate [43].

The crystallite size of carnelian was calculated from the 101 quartz peak using the Scherrer equation (see the Methods section) that yielded values of 434–542 Å for samples from Stirling Brook and 228–333 Å from Green Brook (Table 2). Calculation of the crystal microstrain (lattice dislocations and point defects; see the Methods section) reveals a similar variation between the two locations, with lower values of 0.078–0.098 in samples from Stirling Brook compared to values of 0.126–0.184 in samples from Green Brook (Table 2). Variation in the crystallite size between the Stirling Brook and Green Brook samples is not due to differences in the temperature or pH of the mineralizing fluid or the age of the samples because the geochemical data indicate that precipitation occurred under comparable conditions, and the field relationships imply that their formation was roughly contemporaneous. We interpret variation in the crystallite size of the samples as a result of the moganite content and amount of lattice microstrain. Moganite is metastable and transforms into a more stable α -quartz through dissolution and loss of internal water as it recrystallizes [43]. Its transformation is also enhanced by decreases in the amount of silica in the fluid and in the amount of lattice defects present [44]. All carnelian samples have similar values of SiO_2 , so this is probably not a factor, but samples from Green Brook have a higher percent of lattice microstrain (Table 2). A correlation between the broadening of the

100 quartz peak at $\sim 20^\circ 2\theta$ and the increased amount of moganite was found by [45]. Peak broadening in all varieties of microfibrous quartz is also attributed to small crystallite size and increased lattice microstrain [46]. Carnelian from Green Brook displays a broadened peak width (Figure 6) that is consistent with higher amounts of moganite and lattice microstrain compared to the samples from Stirling Brook.

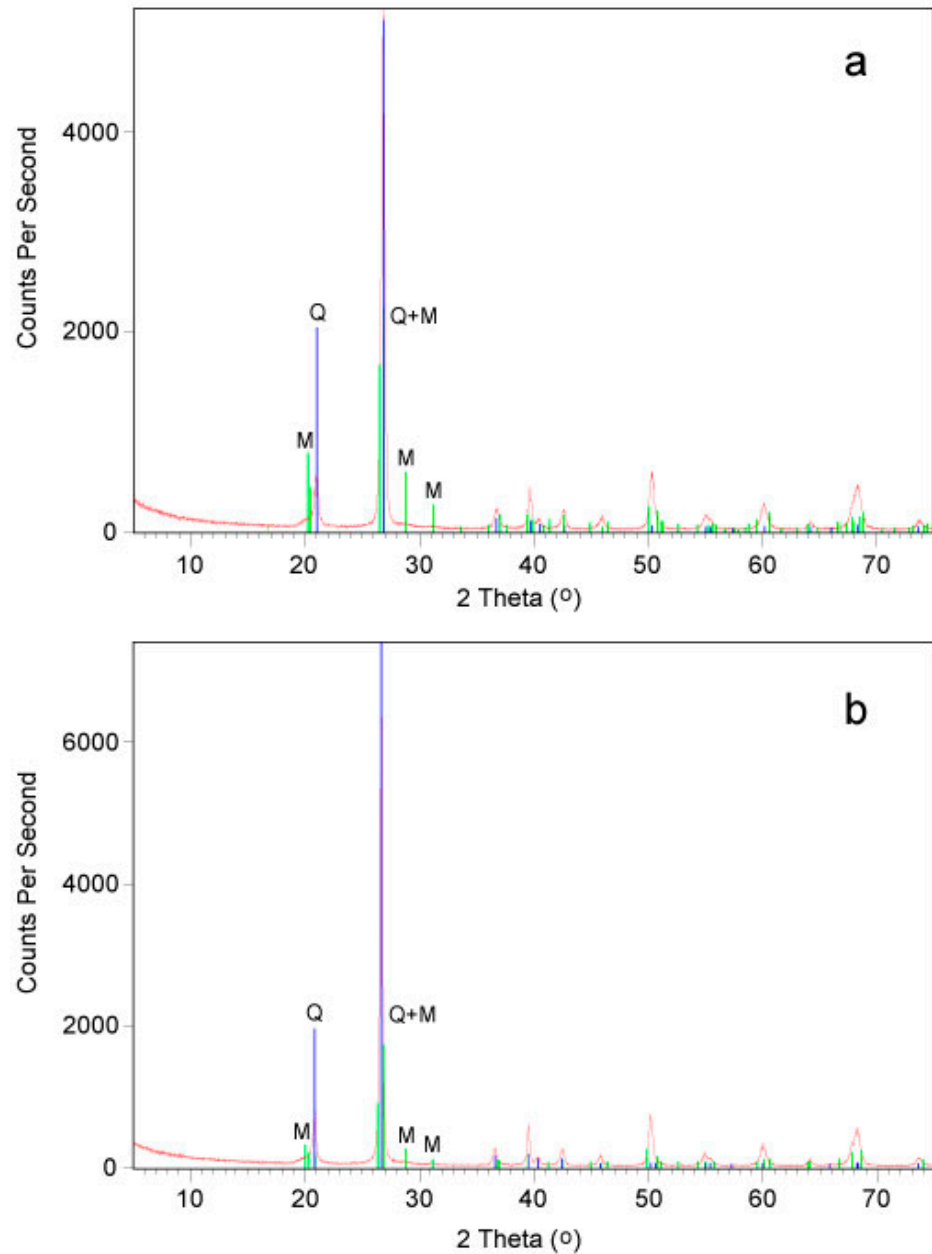


Figure 6. X-ray diffraction patterns of carnelian from New Jersey. (a) Sample GBR 1 from Green Brook. (b) Sample SGB 1 from Stirling Brook. The principal index peaks of quartz (Q) are shown in blue and moganite (M) is shown in green.

Table 2. Characterization of crystallite size and microstrain from the 101 peaks of the carnelian samples from Green Brook (GBR) and Stirling Brook (SGB).

| Sample | Position °2 θ | FWHM °2 θ | C _(s) Å | Lattice Strain % |
|--------|----------------------|------------------|--------------------|------------------|
| GBR-1 | 26.638 | 0.3346 | 255 | 0.165 |
| GBR-2 | 26.805 | 0.2558 | 333 | 0.126 |
| GBR-3 | 26.644 | 0.3739 | 228 | 0.184 |
| SGB-1 | 26.635 | 0.1968 | 434 | 0.098 |
| SGB-2 | 26.633 | 0.1574 | 542 | 0.078 |

FWHM, full width at half maximum of the peak; C_(s), crystallite size.

4.5. Geochemistry

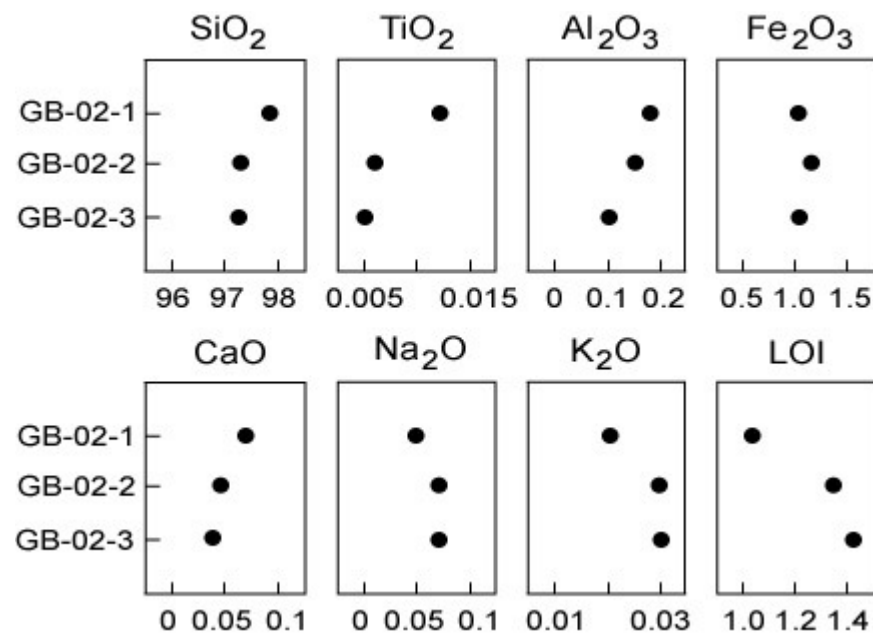
The geochemical analyses of the carnelian samples are provided in Table 3. Major elements are dominated by SiO₂ and Fe₂O₃, which average 97.51 ± 0.31 and 1.09 ± 0.07 wt.%, respectively. Loss on ignition (LOI) is also high and averages 1.27 ± 0.21 wt.%. Elements such as Al₂O₃ and TiO₂ that readily substitute for Si in the quartz structure are quite low, averaging <0.2 and <0.01 wt.%, respectively, as are the rest of the major elements that are present in amounts <0.07 wt.% (Figure 7). Abundances of transition elements all fall below the analytical detection limits. Values of most other trace elements are low except for Y (5–94 ppm), Nb (68–260 ppm), Ta (14–51 ppm), W (5–19 ppm), Th (8–48 ppm), and U (14–77 ppm). The REE are present in amounts above detection limits, and total REE abundances (Σ REE) range from 15 to 85 ppm. Chondrite-normalized REE patterns are parallel and display a progressive increase from La to Lu that differs markedly from average Preakness Basalt and gabbroid (Figure 8a). All of the samples are significantly enriched in heavy REE (HREE) relative to light REE (LREE) (Figure 8a) and have (La/Yb)_N of 0.01–0.02, (La/Sm)_N of 0.05–0.12, and a (Gd/Yb)_N of 0.11–0.60, normalized to chondrite. The samples have large negative Eu anomalies of 0.020–0.026 and nominal Ce anomalies of 0.87–1.01 (Table 3). Yttrium is fractionated from Ho in all samples and displays negative anomalies in two samples (Y/Ho = 3.9–7.9) and a small positive anomaly in the third (Y/Ho = 29.4) compared to chondrite and MORB that have Y/Ho of 27.7 [47]. Abundances of incompatible elements normalized to the upper continental crust display similar patterns that are characterized by negative anomalies of Rb, Ba, La, Sr, and Ti and positive anomalies of Th, U, Nb, and Ta (Figure 8b). The very low values of CaO and Sr in the carnelian are consistent with the absence of associated carbonate minerals.

Numerous investigations have shown that the red color of chalcedony, and by extension carnelian, is attributed to inclusions of Fe-oxide/hydroxide minerals [48,49], and more specifically to hematite [44,50]. Studies involving spectroscopic analysis of agate reveal a correlation between increased hematite concentrations in layers colored red or reddish-orange and increased goethite concentrations in those colored yellow [44]. We propose that the presence of hematite and/or goethite are responsible for the predominant red and less common yellow color, respectively, in the New Jersey carnelian. The presence of rutile is dismissed because of the extremely low values of TiO₂ (Table 3).

Table 3. Major and trace element concentrations of the carnelian samples from Green Brook.

| Sample | GBR-02-1 | GBR-02-2 | GBR-02-3 | Sample | GBR-02-1 | GBR-02-2 | GBR-02-3 |
|--------------------------------|----------|----------|----------|--------|----------|----------|----------|
| SiO ₂ (wt.%) | 97.86 | 97.37 | 97.29 | La | 0.76 | 0.35 | 0.09 |
| TiO ₂ | 0.012 | 0.006 | 0.005 | Ce | 3.65 | 2.02 | 0.58 |
| Al ₂ O ₃ | 0.18 | 0.15 | 0.10 | Pr | 0.82 | 0.57 | 0.14 |
| Fe ₂ O ₃ | 1.06 | 1.18 | 1.04 | Nd | 4.69 | 4.46 | 0.71 |
| MnO | 0.013 | 0.014 | 0.012 | Sm | 3.90 | 4.64 | 0.67 |
| MgO | 0.01 | 0.01 | 0.01 | Eu | 0.033 | 0.04 | 0.005 |
| CaO | 0.07 | 0.04 | 0.03 | Gd | 3.82 | 7.92 | 0.68 |
| Na ₂ O | 0.05 | 0.07 | 0.07 | Tb | 1.69 | 2.06 | 0.28 |
| K ₂ O | 0.02 | 0.03 | 0.03 | Dy | 15.60 | 15.30 | 2.64 |
| P ₂ O ₅ | 0.01 | 0.01 | 0.01 | Ho | 3.74 | 3.19 | 0.59 |
| LOI | 1.03 | 1.36 | 1.41 | Er | 14.10 | 9.99 | 2.47 |
| Total | 100.31 | 100.24 | 100.01 | Tm | 3.21 | 1.55 | 0.556 |
| Ga (ppm) | 2.0 | 1.0 | 1.0 | Yb | 25 | 10.50 | 5.09 |
| Ge | 0.9 | 4.6 | 2.9 | Lu | 3.98 | 1.44 | 0.768 |
| Rb | 1.0 | 1.0 | 1.0 | Hf | 1.5 | 0.2 | 0.3 |
| Sr | 4.0 | 3.0 | 3.0 | Ta | 51.1 | 41.4 | 14.4 |
| Y | 14.6 | 93.9 | 4.7 | W | 18.7 | 5.1 | 5.8 |
| Zr | 19 | 4.0 | 6.0 | Pb | 15 | 32 | <5.0 |
| Nb | 260 | 158 | 68.3 | Th | 48.2 | 19.9 | 7.94 |
| Sn | 5.0 | 1.0 | 1.0 | U | 76.6 | 30.9 | 13.7 |
| Sb | <0.2 | <0.2 | 0.2 | ΣREE | 84.99 | 64.03 | 15.27 |
| Ba | 19 | 12 | 11 | Ce/Ce* | 1.00 | 0.87 | 1.01 |
| Sr | 4.0 | 3.0 | 3.0 | Eu/Eu* | 0.026 | 0.020 | 0.023 |

Fe₂O₃, total iron as Fe₂O₃; LOI, loss on ignition. Ce/Ce* = 2Ce_N/(La_N + Pr_N); Eu/Eu* = Eu_N/[(Sm_N + Gd_N)/2], normalized to chondrite values of [51].

**Figure 7.** Plots of major element abundances (wt.%) in carnelian from Green Brook. Sample numbers are keyed to Table 3.

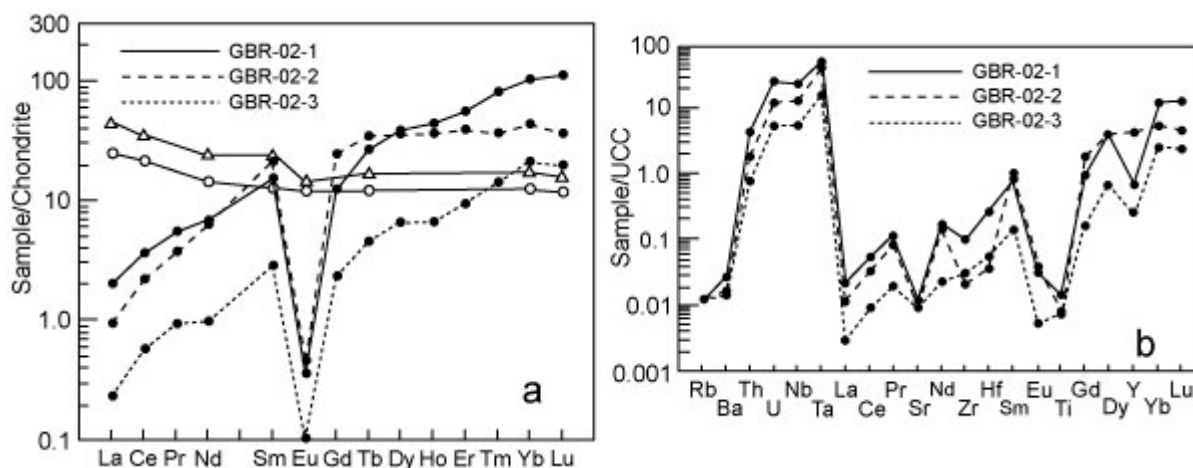


Figure 8. (a) Chondrite-normalized REE patterns of carnelian from Green Brook (solid circles) compared to Preakness Basalt (open circles) and Preakness gabbroid (open triangles). REE normalization values are from [51]. Basalt and gabbroid data are from [32]. (b) Upper continental crust-normalized multielement diagram of carnelian from Green Brook. Normalization values are from [52].

4.6. Oxygen Isotopes

Oxygen isotope analyses of carnelian samples yield high $\delta^{18}\text{O}_{\text{VSMOW}}$ values that range from +18.3 to +31.2‰ (Table 4), with all but one sample having an $\delta^{18}\text{O}$ of +27.9 to +31.2‰. The analytical precision (1σ) is $\pm 0.06\text{‰}$ in two samples and ± 0.21 to 0.64‰ in the other four (Table 4) compared to $\pm 0.1\text{‰}$ for the standards, indicating isotopic heterogeneity, particularly in GBR-3 and GBR-4. The reasons for this heterogeneity between the samples are discussed later in this paper (see Section 5.3). It is noteworthy that no correlation was observed between the $\delta^{18}\text{O}$ of the samples and their geographic location or their color.

Our data fall within the range of oxygen isotope values of chalcedony hosted by volcanic rocks globally (Figure 9). Because of the paucity of published mineralogical studies of carnelian, it was necessary to compare our $\delta^{18}\text{O}$ data to global occurrences of basalt-hosted chalcedony and/or agate, examples of which include the following. $\delta^{18}\text{O}$ values of +22.1 to +28.8‰ are reported from agate in Jurassic quartz latite in Namibia [53]. Chalcedony from the Jurassic Karoo basalt in South Africa yielded $\delta^{18}\text{O}$ values of +20.1 to +21.2‰ [54]. Agate hosted by Eocene to Miocene volcanic rocks in Iran provided $\delta^{18}\text{O}$ values of +23.8 to +26.6‰ [55]. $\delta^{18}\text{O}$ values of +24.5 to +30.3‰ are reported from agate in the Cretaceous Paraná basalt in Brazil [56], similar to $\delta^{18}\text{O}$ of +21.2 to +31.1‰ from amethyst geodes in the same basalt in Uruguay [57], with early formed chalcedony typically occupying the upper end of this range. $\delta^{18}\text{O}$ values of +16.4 to +33.4‰ were obtained from agate occurrences globally in a variety of felsic and mafic host rocks [47,58]. The variation of $\sim 10\text{‰}$ in the $\delta^{18}\text{O}$ values of our study is, therefore, not unusual compared to the similar range of values of other studies.

Table 4. Oxygen isotope results of carnelian from Green Brook.

| Sample (# of Analyses) | Color | $\delta^{18}\text{O}$ (‰ VSMOW) | Std. Dev. (1σ) | Meteoric Water (°C) | Seawater (°C) | Magmatic Fluid (°C) |
|---------------------------|------------|------------------------------------|----------------------------|------------------------|------------------|------------------------|
| GBR-1 (n = 1) | Red | +28.9‰ | — | 28 | 50 | 100 |
| GBR-2 (n = 2) | Red | +31.2‰ | 0.21 | 19 | 39 | 82 |
| GBR-3 (n = 2) | Red-orange | +29.9‰ | 0.56 | 24 | 45 | 92 |
| GBR-4 (n = 2) | Red-orange | +27.8‰ | 0.64 | 32 | 56 | 108 |
| GBR-5 (n = 3) | Yellow | +18.3‰ | 0.06 | 82 | 121 | 223 |
| GBR-6 (n = 3) | Yellow | +30.5‰ | 0.06 | 21 | 42 | 88 |

Calculated formation temperatures (°C) based on $\delta^{18}\text{O}$ of meteoric water (−5‰), seawater (0‰), and magmatic fluid (+8‰). See text for details.

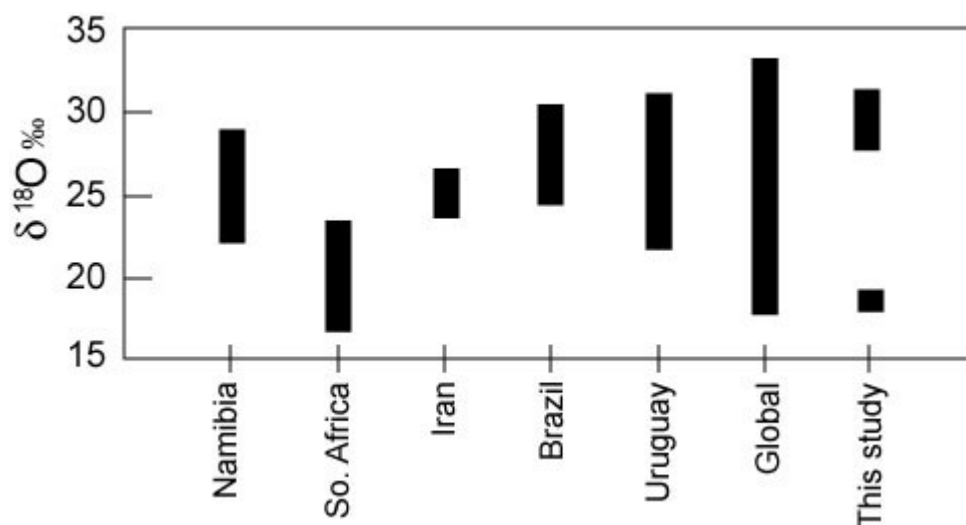


Figure 9. A plot of the $\delta^{18}\text{O}$ values of New Jersey carnelian compared to global occurrences of basalt-hosted chalcedony, agate [48,53,55–57], and carnelian [54].

5. Discussion

5.1. Source of Elements in Carnelian

Most trace elements and REE, with the exception of Ga, Ge, and B, are unable to be structurally incorporated into the Si lattice and are incorporated in micro-inclusions in quartz or are adsorbed onto its surface [59]. Therefore, concentrations of trace elements and REE in the carnelian of this study provide important insights into the source of these elements. Nearly all trace elements and REE abundances differ from those in Preakness Basalt or gabbroid (Figure 8). In particular, Preakness Basalt and gabbroid contain much lower abundances of Th (2.0 ppm), Nb (4.2 ppm), and Ta (0.35 ppm) [33] compared to the values in carnelian (Table 3). Also of note are the high values of W and U in the carnelian (5–19 ppm and 14–76 ppm, respectively). Although W and U are not reported for mafic igneous rocks of the Newark basin, these values are typically low in basalt, averaging 0.01–0.09 ppm W and 0.05–0.18 ppm U in mid-ocean-ridge basalt and 0.56 ppm W and 1.02 ppm U in ocean island basalt [47].

In New Jersey, trace element values that are comparable to those in the carnelian are found only in granulite to amphibolite facies Mesoproterozoic rocks and/or greenschist facies Neoproterozoic rocks of the exposed New Jersey Highlands and their buried segments beneath the Newark basin. Widespread and abundant Mesoproterozoic felsic orthogneiss and paragneiss have high REE abundances and as much as 214 ppm U, 650 ppm Th, 100 ppm Nb, 7.0 ppm Ta, and 4.0 ppm W, [60,61], and regionally abundant Mesoproterozoic low-Ti magnetite deposits locally contain elevated abundances of U, Th, and REEs [62–64]. Additionally, Neoproterozoic hematitic ironstone deposits contain as much as 100 ppm U, 45 ppm Th, and 300 ppm W [65]. Elevated Fe abundances in the carnelian were likely sourced from various Proterozoic lithologies and/or ore deposits that oxidized Fe^{2+} to Fe^{3+} under near-surface conditions. The leaching of Fe-rich Mesoproterozoic lithologies at depth by hydrothermal fluids is shown to be the source of Fe and other metals in the Neoproterozoic ironstone deposits in New Jersey [65]. Although high field strength elements are often considered to be immobile, they are shown to have increased solubility in acidic fluids or fluids containing Cl and F [66–68]. Halogens are particularly abundant in Mesoproterozoic orthogneiss that contains Cl in amphibole and widespread occurrences of scapolite, whereas F is present in fluorapatite, which is commonly found in the numerous regional magnetite deposits.

For these reasons, we interpret Proterozoic rocks to be the likely source for the elevated abundance of most elements in the carnelian. This means that during the Jurassic, certain physicochemical conditions existed, such as extensional brittle faults that would have permitted ascending fluids to egress to the Preakness, as well as deeply circulating heated

fluids capable of enhancing mineral solubility and mobilizing elements from basement lithologies. The first condition is met by the presence of intrabasinal extensional faults that were active during the Triassic and Jurassic and references therein [69]. The second condition is supported by the downward flow of meteoric water during the Triassic and Jurassic along the border fault separating the Proterozoic rocks from the Newark basin (Figure 1), followed by convective circulation and ascent as hydrothermal fluid at temperatures of 150–280 °C [70] and 137–232 °C [71] from fluid inclusion studies of anhydrite and calcite, respectively, and 100–250 °C from zircon and apatite fission-track analysis [72].

The source of silica in the carnelian is less straightforward, and sources external or internal to the Preakness were considered. Silica is a major component of siliceous sinters formed in a terrestrial hot spring/geyser environment. However, these deposits are mainly composed of some combination of opal-A, opal-CT, opal-C, and macroscopic quartz that typically lack an association with chalcedony [73,74] or do not directly precipitate chalcedony [75]. Opal is absent in all samples of New Jersey carnelian and features consistent with a siliceous sinter, such as those observed in Orange Mountain Basalt [38], are not recognized in the Preakness.

Silica may have been derived through the partial dissolution of detrital quartz grains in the underlying Feltville Formation by alkaline fluids. These reddish-brown clastic rocks are rich in quartz and contain abundant hematite that coats detrital grains and occurs in the rock matrix. A similar interpretation was made for silicified sand layers at the tops of flows in the Paraná continental flood basalt formed from the fluidization of sand in the underlying Botucatu Formation that was transported in ~150 °C hydrothermal fluids [76,77]. The injection of fluidized sand into the Preakness as dikes, sills, or veins would have left remnant patches of non-bedded sediment or sediment-filled fractures in the basalt, which are not observed. Alternatively, the dissolution of detrital quartz grains may have released silica that reacted to form silicic acid, precipitating carnelian in the Preakness as the fluid became silica saturated and leaving no sediment residue. This would have taken place under conditions of higher temperature than cool surface water and at pH > 4 necessary for the solubility of silica [37,78].

We favor the devitrification of abundant glass in the gabbroid of the Preakness first flow as the source of silica in the carnelian for the following reasons. Silica-saturated fluids may readily form through the hydrolysis of highly reactive basaltic glass by acidic fluids [37,79]. The breakdown of interstitial glass in the basalt of the Paraná volcanic province was posited as the source of silica that filled large amethyst geodes there [80,81], and the alteration of basalt by a heated fluid is interpreted to be the source of silica in agate in Cuba [82]. Numerous studies of basaltic glass alteration document initial losses in Al₂O₃, MgO, CaO, Na₂O, and K₂O [83–86]. Glass-rich gabbroid in the Preakness displays comparable depletions of up to 4.0 wt.% Al₂O₃, 3.0 wt.% MgO, 3.0 wt.% CaO, and 0.7 wt.% K₂O compared to host Preakness Basalt (Table 1). The fact that carnelian is not found in, or associated with, the Preakness elsewhere in the Newark basin demands that unique conditions must have existed in the study area. We propose that these conditions are a result of the occurrence of the thickest gabbroid bodies recorded in the Preakness that contain a considerable volume of basaltic glass available to supply the silica. Although gabbroid bodies are recognized in the Preakness at other locations, they are much thinner, and the same physicochemical conditions that were present in the study area were not duplicated elsewhere in the Newark basin.

5.2. Movement and Timing of Mineralizing Fluid

We evaluated pathways in the Preakness that were most likely to have controlled the movement of fluid from which carnelian formed. Typical fine-grained basalt in the first flow is sparsely vesicular, with vesicles comprising <0.2 volume% of the rock [26]. The lowest part of this flow is characterized by slender and vertical columnar joints that would have permitted fluid to ascend along a subvertical path during the cooling of the flow. Fluid infiltrating the Preakness may have also utilized intrabasinal extensional faults that were

active throughout the evolution of the Newark basin [69] and that are common in the study area as steeply dipping (70–90°), mainly open, and unmineralized brittle faults as wide as 0.5 m [33]. Although it is possible that silica-saturated fluid utilized these pathways, the preservation of vesicle molds on the lower surfaces of some carnelian is not compatible with its precipitation along columnar joints or faults, which lack amygdaloidal features.

Degassing of the volatile phases during the cooling of the Preakness must have been fairly rapid because gas bubbles had insufficient time to form vesicles or coalesce into larger vugs or openings in the lower or middle parts of the first flow. The reduced water–rock interaction also likely explains why this part of the first flow is relatively unaltered and has low values of LOI (Table 1). By contrast, thick gabbroid bodies in the upper part of the first flow contain 3 m thick intervals in which vesicles with diameters of 2–10 mm comprise as much as 19% of the volume of the rock [26], indicating that gabbroid formed a barrier and trapped rising gas bubbles. Gabbroid also preserves petrographic and geochemical features compatible with hydrothermal alteration, which suggests that it had ample opportunity to interact with heated fluid. These include gains in Na₂O due to the albitization of plagioclase, a loss of CaO and Sr that reflect plagioclase alteration, and high values of LOI that range from 1.8 to 2.5 wt.% (Table 1), indicative of precipitation of secondary hydrous minerals. The evidence for hydrothermal fluid movement in the upper part of the first flow is more consistent with the ascent of a heated, syn-eruptive fluid than with infiltration of the basalt by a low-temperature post-eruptive fluid. Thus, we propose that it was in the altered, volatile-rich upper part of the first flow that carnelian most probably precipitated.

The absence of any dateable material in the carnelian renders the timing of its formation to be a challenge. Therefore, we relied on indirect evidence, such as the presence of glauberite molds in some pieces. Studies of the paragenesis of secondary mineralization in basalt formations of the Newark basin indicate that crystallization of the basalt and precipitation of contemporaneous saline minerals were closely followed in time by the albitization of plagioclase and the precipitation of abundant silica [17,21]. The precipitation of carnelian in the Preakness first flow containing glauberite (Figure 4c) is consistent with this paragenetic sequence, suggesting that carnelian may have formed contemporaneously with the crystallization of the Preakness at 201 Ma.

5.3. Characteristics of the Mineralizing Fluid

Multiple lines of evidence provide insights into the temperature, composition, and pH of the fluid from which carnelian formed. One constraint on the syn- to post-depositional thermal history of the Newark basin is provided by geochemical analysis of thermally mature hydrocarbons in the Feltville Formation from beneath the Preakness Basalt that indicate a burial temperature of 90–130 °C [87]. Using this ~100 °C estimate from burial constraints, carnelian samples with $\delta^{18}\text{O}$ of +27.9 to +31.1‰ would be in isotopic equilibrium with water having $\delta^{18}\text{O}$ of +7 to +10‰ when calculated using the fractionation factor for α -quartz of [88]. If correct, this calculation would indicate that pure magmatic water ($\delta^{18}\text{O}$ of ~+8‰) precipitated these carnelian samples. Although Preakness gabbroid preserves evidence compatible with hydrothermal alteration, we do not think the oxygen isotope ratios reflect the formation of the carnelian strictly from a high-temperature (>100 °C) magmatic fluid because calculations at higher temperatures yield unrealistic water $\delta^{18}\text{O}$ values, and also because higher temperatures are not supported by the extremely low values of Ti in our samples. Furthermore, in a cooling volcanic system, magmatic fluid commonly mixes with surface water, producing lower fluid $\delta^{18}\text{O}$ values.

To explore possible fluid sources, we calculated formation temperatures for the carnelian from end-member fluid compositions (Table 4). Meteoric water for the ~20° paleolatitude of the Newark basin at about 200 Ma [89] is estimated to have been ca. –5‰ using modern latitude versus $\delta^{18}\text{O}$ relationships [90]. If water with $\delta^{18}\text{O}$ of –5‰ precipitated the higher- $\delta^{18}\text{O}$ carnelian samples, then the equilibrium formation temperatures would have been 19–32 °C. The calculated temperatures using a fluid of seawater composition ($\delta^{18}\text{O} \approx 0\text{‰}$) are 40–55 °C. Seawater may be a viable proxy for a minor component of a

brine-like fluid that precipitated glauberite in the Preakness first flow. The upper range of temperatures calculated using only magmatic fluid with $\delta^{18}\text{O}$ of +8‰ is 82–108 °C. If the $\delta^{18}\text{O}$ of +18.3‰ in the carnelian sample GBR-5 is included, the maximum temperatures are higher and range from 82–223 °C. The lower $\delta^{18}\text{O}$ value of GBR-5 more likely reflects a combination of differences in temperature and different fluid or fluid mixtures compared to the other samples. We interpret the formation temperatures for the carnelian in this study to fall mainly in the range of 20–80 °C based on calculations using meteoric water and magmatic (hydrothermal) fluid. A more precise estimate requires knowledge of the proportion of the different fluids involved in mixing, but even then, the maximum temperature would probably not have been much above ~100 °C. Regardless, the formation temperature would not have remained high for very long because chalcedony precipitates from silica-saturated fluids that cool fairly rapidly, with slow cooling favoring the crystallization of macrocrystalline quartz [37].

In terms of the fluid composition, variations in the $\delta^{18}\text{O}$ values and geochemical characteristics of the carnelian are most reasonably explained by the mixing of a deeper, higher-temperature hydrothermal fluid and shallower, lower-temperature meteoric water, with variations in these parameters due mainly to differences in the ratio of the fluids. This interpretation is in agreement with [71], who proposed the mixing of heated basement-derived fluid and cooler formational water to be responsible for the precipitation of calcite in veins in Triassic sedimentary rocks in the Newark basin. Our results expand the effects of fluid mixing to include the Jurassic part of the Newark basin and also account for the precipitation of silica mineralization.

We interpret the deep circulating hydrothermal fluid as having been acidic and responsible for mobilizing trace elements from the Proterozoic basement. Total REE abundances are higher in acidic fluids than alkaline fluids [78], and the mobilization of REE also increases when complexed by F- or Cl-rich fluids [66,68]. Such fluids are more strongly enriched in HREE ($\text{La}/\text{Yb}_\text{N} \ll 1$), comparable to the values of our study ($\text{La}/\text{Yb}_\text{N} = 0.01\text{--}0.02$). In contrast, the shallower meteoric fluid was more likely to have been alkaline. Changing conditions of pH from acidic to alkaline are evidenced in the carnelian geochemistry of samples GBR-02-1 through GBR-02-3. These samples display a progressive decrease in ΣREE (85 to 15 ppm), HREE (50 to 9.5 ppm), Nd + Yb (30 to 6 ppm), and Nb, Ta, and W (Table 3). Studies show that decreases in these elements are attributed to an increase in pH [78,91–93]. The enrichment in HREEs in all of the carnelian samples may result from the increased solubility of HREE over LREEs in hydrothermal fluids under conditions of a neutral to slightly alkaline pH of 6.3–9 [93,94]. Additionally, the adsorption of HREE onto the large surface area of Fe oxide/hydroxide is greater at pH < 8 [93] and is especially significant at a pH of 6.5–8 [78]. Uranium is mobile as U^{VI} at a neutral to alkaline pH of 7–9 and readily adsorbs onto quartz surfaces or in structural sites in quartz [95,96]. Uranium and Th also readily adsorb onto Fe oxides/hydroxides at a pH of 6–9 [78,92,93,97]. The presence of moganite in our carnelian samples is also noteworthy because moganite precipitates from alkaline fluids containing ferric iron [42]. These results, in combination with the data of our study, support the precipitation of carnelian under conditions of a neutral to slightly alkaline pH.

6. Conclusions

Carnelian in New Jersey is recognized from only a few closely spaced locations in the Mesozoic Newark basin. Although carnelian has yet to be observed in situ in bedrock outcrops, we present evidence that supports its precipitation in coarse-grained gabbroid layers in the Lower Jurassic Preakness Basalt roughly contemporaneous with the crystallization of the basalt at 201 Ma. Erosion of the host rock continues to concentrate carnelian in proximal deposits of fluvial gravel, colluvium, and alluvium.

Carnelian is composed of length-fast chalcedony characterized by fibrous bundles overlain by wavy extinction bands. XRD patterns exhibit peaks that are characteristic of α -quartz and minor moganite (>5%). Major element abundances are dominated by SiO_2

(97.5 ± 0.31 wt.%) and Fe_2O_3 (1.09 ± 0.07 wt.%); Al_2O_3 and TiO_2 are low, averaging < 0.2 and < 0.01 wt.%, respectively, and the rest of the major elements are < 0.07 wt.%. Silica was derived through the devitrification of abundant volcanic glass in coarse-grained gabbroid layers in the upper part of the Preakness first flow. Trace element concentrations are low except for Y, Nb, Ta, Pb, W, Th, and U. We show that most trace elements were likely sourced from Proterozoic lithologies. REE display parallel chondrite-normalized patterns that are enriched in HREE relative to LREE and have large negative Eu anomalies (0.02). $\delta^{18}\text{O}$ values of carnelian are high and range from $+18.3$ to $+31.2$ ‰, with all but one sample having an $\delta^{18}\text{O}$ of 29.9 ± 1.3 ‰.

The results of this study are consistent with the formation of carnelian mainly from a mixture of higher-temperature hydrothermal fluid and shallower, lower-temperature, meteoric water. Variations in the $\delta^{18}\text{O}$ values and geochemical characteristics of carnelian are due to differences in the ratio of these fluids. Carnelian precipitated under conditions of neutral to slightly alkaline pH and relatively low temperatures of 20 – 80 °C, which is comparable to other global occurrences of volcanic rock-derived chalcedony.

Author Contributions: Conceptualization—R.A.V. and S.D.S.; methodology—M.L.G., W.H.P. and R.A.V.; formal analysis—M.L.G. and W.H.P.; writing—original draft, R.A.V. and S.D.S.; writing—review and revisions, M.L.G. and W.H.P. All authors have read and agreed to the published version of the manuscript.

Funding: This research received no external funding.

Data Availability Statement: The data presented in this study are contained within the article.

Acknowledgments: Justin Dodd and Anna Buczynska are thanked for performing the oxygen isotope analyses at Northern Illinois University. We are grateful to the two anonymous reviewers whose comments improved the quality of the paper.

Conflicts of Interest: The authors declare no conflict of interest.

References

- Francis, P., Jr. The stone bead industry of southern India. *Beads* **2000**, *12*, 49–62.
- Brunet, O. Bronze and Iron Age carnelian bead production in the UAE and Armenia: New perspectives. *Proc. Semin. Arab. Stud.* **2009**, *39*, 57–68.
- Charpentier, V.; Brunet, O.; Méry, S.; Velde, C. Carnelian, agate, and other types of chalcedony: The prehistory of Jebel al-Ma'taradh and its semiprecious stones, Emirate of Ra's al-Khaimah. *Arab. Arch. Epig.* **2017**, *28*, 175–189. [[CrossRef](#)]
- Geological Survey of India. *Geology and Mineral Resources of Gujarat, Daman and Diu*; Miscellaneous Publication 30, Part 14; Popular Printers: Jaipur, India, 2012; 85p.
- Malunga, G.W.P. *An Analysis of Mineral Resources of Malawi*; Published in Malawi by the author; 2014; 82p.
- Gliozzo, E.; Mattingly, D.J.; Cole, F.; Artoli, G. In the footsteps of Pliny: Tracing the sources of Garamantian carnelian from Fazzan, south-west Libya. *J. Archaeol. Sci.* **2014**, *52*, 218–241. [[CrossRef](#)]
- Carter, A.K.; Dussubieux, L. Geologic provenience analysis of agate and carnelian beads using laser ablation-inductively coupled plasma-mass spectrometry (LA-ICP-MS): A case study from Iron Age Cambodia and Thailand. *J. Archaeol. Sci. Rep.* **2016**, *6*, 321–331. [[CrossRef](#)]
- Polekhovsky, Y.S.; Punin, Y.O. Agate mineralization in basaltoids of the northeastern Ladoga Region, South Karelia. *Geol. Ore Depos.* **2008**, *50*, 642–646. [[CrossRef](#)]
- Zodac, P. New Jersey Brook a carnelian locality. *Rocks Miner.* **1950**, *25*, 481–483. [[CrossRef](#)]
- Zeitner, J.C. *Appalachian Mineral and Gem Trails*; Arts and Crafts Press: San Diego, CA, USA, 1968; 134p.
- Mason, B.H. *Trap Rock Minerals of New Jersey*; Bulletin 64; Geological Survey of New Jersey: Trenton, NJ, USA, 1960; 51p.
- Peters, J.J. The minerals of Bergen Hill, New Jersey. In *Igneous Rocks of the Newark Basin: Petrology, Mineralogy, Ore Deposits and Guide to Field Trip*; Puffer, J.H., Ed.; Geological Association of New Jersey Field Conference: Trenton, NJ, USA, 1984; pp. 96–102.
- Seymour, E. List of minerals in New Jersey. In *Geology of New Jersey*; Geological Survey of New Jersey: Trenton, NJ, USA, 1868; pp. 743–750.
- Canfield, F.A. Catalogue of minerals found in New Jersey. In *Final Report of the State Geologist*; Geological Survey of New Jersey: Trenton, NJ, USA, 1889; pp. 1–24.
- Valiant, W.S. New Jersey mineral localities. *Min. Coll.* **1904**, *11*, 122–125, 137–141, 150–154.
- Beck, L.C. Notices of some trappen minerals found in New Jersey and New York. *Am. J. Sci.* **1843**, *44*, 54–60.

17. Fenner, C.N. The Watchung Basalt and the paragenesis of its zeolites and other secondary minerals. *Ann. N. Y. Acad. Sci.* **1910**, *20*, 93–187. [\[CrossRef\]](#)
18. Gordon, S.G. A review of the genesis of the zeolite deposits of First Watchung Mountain, N.J.1. *Am. Mineral.* **1916**, *1*, 72–80.
19. Wherry, E.T. The lozenge-shaped cavities in the First Watchung Mountain zeolite deposits. *J. Wash. Acad. Sci.* **1916**, *6*, 181–184.
20. Manchester, J.G. The minerals of the Bergen Archways. *Am. Mineral.* **1919**, *4*, 107–116.
21. Schaller, W.T. *The Crystal Cavities of the New Jersey Zeolite Region*; Bulletin 832; U.S. Geological Survey: Reston, VA, USA, 1932; 90p.
22. Manspeizer, W. Rift tectonics inferred from volcanic and clastic structures. In *Field Studies of New Jersey Geology and Guide to Field Trips*; Manspeizer, W., Ed.; Rutgers University: Newark, NJ, USA, 1980; pp. 314–350.
23. Fedosh, M.S.; Smoot, J.P. A cored stratigraphic section through the northern Newark basin, New Jersey. In *Studies of the Early Mesozoic Basins of the Eastern United States*; Froelich, A.J., Robinson, G.R., Jr., Eds.; Bulletin 1776; U.S. Geological Survey: Reston, VA, USA, 1988; pp. 19–24.
24. Olsen, P.E.; Kent, D.V.; Cornet, B.; Witte, W.K.; Schlische, R.W. High-resolution stratigraphy of the Newark rift basin (early Mesozoic, eastern North America). *Geol. Soc. Am. Bull.* **1996**, *108*, 40–77. [\[CrossRef\]](#)
25. Blackburn, T.J.; Olsen, P.E.; Bowring, S.A.; McLean, N.M.; Kent, D.V.; Puffer, J.; McHone, G.; Rasbury, E.T.; Et-Touhami, M. Zircon U-Pb geochronology links end-Triassic extinction with the Central Atlantic Magmatic Province. *Science* **2013**, *340*, 941–945. [\[CrossRef\]](#)
26. Puffer, J.H.; Volkert, R.A. Pegmatoid and gabbroid layers in Jurassic Preakness and Hook Mountain Basalts, Newark Basin, New Jersey. *J. Geol.* **2001**, *109*, 585–601. [\[CrossRef\]](#)
27. Faust, G.T. *Joint Systems in the Watchung Basalt Flows, New Jersey*; Professional Paper 864-B; U.S. Geological Survey: Reston, VA, USA, 1978; 46p.
28. Kümmel, H.B. The Newark System of New Jersey. In *Annual Report of the State Geologist*; Geological Survey of New Jersey: Trenton, NJ, USA, 1898; pp. 23–159.
29. Lewis, J.V. The pillow lavas of the Watchung Mountains. In *Administrative Report of the State Geologist*; Bulletin 16; Geological Survey of New Jersey: Trenton, NJ, USA, 1915; pp. 51–56.
30. Lewis, J.V. Petrography of the Newark igneous rocks of New Jersey. In *Annual Report of the State Geologist*; Geological Survey of New Jersey: Trenton, NJ, USA, 1908; pp. 97–167.
31. Drake, A.A., Jr.; Volkert, R.A.; Monteverde, D.H.; Herman, G.C.; Houghton, H.F.; Parker, R.A.; Dalton, R.F. *Bedrock Geologic Map of Northern New Jersey*; Misc. Inves. Series Map I-2540-A; U.S. Geological Survey: Reston, VA, USA, 1996.
32. Tollo, R.P.; Hawkins, D.P.; Gottfried, D. *Petrographic and Geochemical Data for Jurassic Basalts from Eight Passaic Tunnel Cores, Newark Basin, New Jersey*; Open-File Report 90-689; U.S. Geological Survey: Reston, VA, USA, 1990; 32p.
33. Monteverde, D.H.; Volkert, R.A. *Bedrock Geologic Map of the Chatham Quadrangle, Morris, Union and Somerset Counties, New Jersey*; GMS 04-02; New Jersey Geological Survey: Ewing Township, NJ, USA, 2005.
34. Sharp, Z.D. A laser-based microanalytical method for the in situ determination of oxygen isotope ratios of silicates and oxides. *Geochim. Cosmochim. Acta* **1990**, *54*, 1353–1357. [\[CrossRef\]](#)
35. Stanford, S.D. *Surficial Geology of the Chatham Quadrangle Morris, Union and Somerset Counties, New Jersey*; OFM 69; New Jersey Geological Survey: Ewing Township, NJ, USA, 2007.
36. Skinner, A.; Schrabisch, M. *A Preliminary Report of the Archaeological Survey of New Jersey*. Bulletin 9; New Jersey Geological Survey: Ewing Township, NJ, USA, 1913; 94p.
37. Fournier, R.O. The behavior of silica in hydrothermal solutions. *Rev. Econ. Geol.* **1985**, *2*, 45–61.
38. Puffer, J.H.; Laskowich, C. Volcanic diapires in the Orange Mountain flood basalt: New Jersey, USA. *J. Volcanol. Geotherm. Res.* **2012**, *237–238*, 1–9. [\[CrossRef\]](#)
39. Stanford, S.D. Onshore record of Hudson River drainage to the continental shelf from the Late Miocene through the late Wisconsin deglaciation, USA: Synthesis and revision. *Boreas* **2010**, *39*, 1–17. [\[CrossRef\]](#)
40. Wherry, E.T. Glauberite crystal-cavities in the Triassic rocks of eastern Pennsylvania. *Am. Mineral.* **1916**, *1*, 37–43.
41. Cady, S.L.; Wenk, H.-R.; Sintubin, M. Microfibrous quartz varieties: Characterization by quantitative X-ray texture analysis and transmission electron microscopy. *Contrib. Mineral. Petrol.* **1998**, *130*, 320–335. [\[CrossRef\]](#)
42. Heaney, P.J. Moganite as an indicator for vanished evaporates: A testament reborn? *J. Sediment. Res.* **1995**, *A65*, 633–638.
43. Moxon, T.; Rios, S. Moganite and water content as a function of age in agate: An XRD and thermogravimetric study. *Eur. J. Mineral.* **2004**, *16*, 269–278. [\[CrossRef\]](#)
44. Zhang, X.; Ji, L.; He, X. Geomological characteristics and origin of the Zhanguohong agate Beipo, Liaoning Province, China: A combined microscopic, X-ray diffraction, and Raman spectroscopic study. *Minerals* **2020**, *10*, 401. [\[CrossRef\]](#)
45. Zhang, M.; Moxon, T. Infrared absorption spectroscopy of SiO₂-moganite. *Am. Mineral.* **2014**, *99*, 671–680. [\[CrossRef\]](#)
46. Graetsch, H.A.; Grünberg, J.M. Microstructure of flint and other chert raw materials. *Archaeometry* **2012**, *54*, 18–36. [\[CrossRef\]](#)
47. Sun, S.S.; McDonough, W.F. Chemical and isotopic systematics of oceanic basalts: Implications for mantle composition and processes. In *Magmatism in the Ocean Basins*; Saunders, A.D., Norry, M.J., Eds.; Special Publication 42; Geological Society of London: London, UK, 1989; pp. 313–345.
48. Götze, J.; Tichomirowa, M.; Fuchs, H.; Pilot, J.; Sharp, Z. Geochemistry of agates: A trace element and stable isotope study. *Chem. Geol.* **2001**, *175*, 523–541. [\[CrossRef\]](#)

49. Pršek, J.; Dumańska-Slowick, M.; Powolny, T.; Natkaniec-Nowak, L.; Tobola, T.; Zych, D.; Skrepnicka, D. Agates from Western Atlas (Morocco)—Constraints from mineralogical and microtextural characteristics. *Minerals* **2020**, *10*, 198. [\[CrossRef\]](#)
50. Dumańska-Slowick, M.; Natkaniec-Nowak, L.; Weselucha-Birczyńska, A.; Gawel, A.; Lankosz, M.; Wróbel, P. Agates from Sidi Rahal, in the Atlas Mountains of Morocco: Geochemical characteristics and proposed origin. *Gems Gemol.* **2013**, *49*, 148–159. [\[CrossRef\]](#)
51. Masuda, A.; Nakamura, N.; Tanaka, T. Fine structures of mutually normalized rare-earth patterns of chondrites. *Geochim. Cosmochim. Acta* **1973**, *37*, 239–248. [\[CrossRef\]](#)
52. Rudnick, R.L.; Gao, S. Composition of the continental crust. In *Treatise on Geochemistry*; Holland, H.D., Turekian, K.K., Eds.; Pergamon: Oxford, UK, 2003; pp. 1–64.
53. Harris, C. Oxygen-isotope zonation of agates from Karoo volcanics of the Skeleton Coast, Namibia. *Am. Mineral.* **1989**, *74*, 476–481.
54. Gliozzo, E.; Cairncross, B.; Vennemann, T. A geochemical and micro-textural comparison of basalt-hosted chalcedony from the Jurassic Drakensberg and Neoproterozoic Ventersdorp Supergroup (Vaal River alluvial gravels), South Africa. *Int. J. Earth Sci.* **2019**, *108*, 1857–1877. [\[CrossRef\]](#)
55. Rezaei-Kahkaei, M.; Ansarifard, O.; Ghasemi, H. Geochemistry and oxygen stable isotopes of Reza Abad agates, SE Shahrood, Central Iran: An approach to temperature and formation process. *J. Econ. Geol.* **2019**, *11*, 525–541. (In Persian)
56. Fallick, A.E.; Jocely, J.; Hamilton, P.J. Oxygen and hydrogen stable isotope systematics in Brazilian agates. In *Geochemistry and Mineral Formation in the Earth Surface*; Rodriguez-Clemente, R., Taedy, Y., Eds.; Centre Nationale de la Recherche Scientifique: Paris, France, 1987; pp. 99–117.
57. Duarte, L.C.; Hartmann, L.A.; Ronchi, L.H.; Berner, Z.; Theye, T.; Massonne, H.J. Stable isotope and mineralogical investigation of the genesis of amethyst geodes in the Los Catalanes gemological district, Uruguay, southernmost Paraná volcanic province. *Miner. Depos.* **2011**, *46*, 239–255. [\[CrossRef\]](#)
58. Götze, J.; Möckel, R.; Pan, Y. Mineralogy, Geochemistry and Genesis of Agate—A review. *Minerals* **2020**, *10*, 1037. [\[CrossRef\]](#)
59. Götze, J.; Pan, Y.; Müller, A. Mineralogy and mineral chemistry of quartz; A review. *Min. Mag.* **2021**, *85*, 639–664. [\[CrossRef\]](#)
60. Volkert, R.A.; Drake, A.A., Jr. *Geochemistry and Stratigraphic Relations of Middle Proterozoic Rocks of the New Jersey Highlands*; Professional Paper 1565-C; U.S. Geological Survey: Reston, VA, USA, 1999; 77p.
61. Volkert, R.A.; Feigenson, M.D.; Patino, L.C.; Delaney, J.S.; Drake, A.A., Jr. Sr and Nd isotopic compositions, age and petrogenesis of A-type granitoids of the Vernon Supersuite, New Jersey Highlands, USA. *Lithos* **2000**, *50*, 325–347. [\[CrossRef\]](#)
62. Klemic, H.; Heyl, A.V., Jr.; Taylor, A.R.; Stone, J. *Radioactive Rare-Earth Deposit at Scrub Oaks Mine, Morris County, New Jersey*; Bulletin 1082-B; U.S. Geological Survey: Reston, VA, USA, 1959; pp. 29–59.
63. Vassiliou, A.H. Uranium and rare earth mineralization at the Bemco mine near Cranberry Lake, New Jersey. In *Field Studies of New Jersey Geology and Guide to Field Trips*; Manspeizer, W., Ed.; New York State Geological Association: Oswego, NY, USA, 1980; pp. 192–199.
64. Baillieu, T.A.; Indelicato, G.J. Uranium in the New Jersey and New York Highlands of the Reading Prong. *Econ. Geol.* **1981**, *76*, 167–171. [\[CrossRef\]](#)
65. Volkert, R.A.; Monteverde, D.H.; Gates, A.E.; Frieauf, K.C.; Dalton, R.F.; Smith, R.C., II. Geochemistry and origin of Neoproterozoic ironstone deposits in the New Jersey Highlands and implications for the Iapetan rifted margin in the north-central Appalachians. In *From Rodinia to Pangea: The Lithotectonic Record of the Appalachian Region*; Tollo, R.P., Bartholomew, M.J., Hibbard, J.P., Karabinos, P.M., Eds.; Memoir 206; The Geological Society of America: Boulder, CO, USA, 2010; pp. 283–306.
66. Jiang, S.-Y.; Wang, R.-C.; Wu, X.-S.; Zhao, K.-D. Mobility of high field strength elements (HFSE) in magmatic-, metamorphic-, and submarine-hydrothermal systems. *Phys. Chem. Earth* **2005**, *30*, 1020–1029. [\[CrossRef\]](#)
67. Bobos, I.; Gomes, C. Mineralogy and geochemistry (HFSE and REE) of the present-day acid-sulfate types alteration from the active hydrothermal system of Furnas Volcano, São Miguel Island, The Azores Archipelago. *Minerals* **2021**, *11*, 335. [\[CrossRef\]](#)
68. Németh, N.; Kristály, F.; Balassa, C. Hydrothermal high field strength element enrichment in the Bükk Mts. (NE Hungary). *J. Geochem. Explor.* **2023**, *246*, 107159. [\[CrossRef\]](#)
69. Withjack, M.O.; Schlische, R.W.; Malinconico, M.L.; Olsen, P.E. Rift-basin development: Lessons from the Triassic-Jurassic Newark Basin of eastern North America. In *Conjugate Divergent Margins*; Mohriak, W.U., Danforth, A., Post, P.J., Brown, D.E., Tari, G.C., Nemčok, M., Sonha, S.T., Eds.; Special Publications 369; The Geological Society: London, UK, 2013; pp. 301–321.
70. El-Tabakh, M.; Riccioni, R.; Schreiber, B.C. Evolution of Late Triassic rift basin evaporites (Passaic Formation): Newark basin, eastern North America. *Sedimentology* **1997**, *44*, 767–790. [\[CrossRef\]](#)
71. Rddad, L.; Kraemer, D.; Walter, B.F.; Darling, R.; Cousens, B. Unraveling the fluid flow evolution and precipitation mechanisms in calcite veins in relation to Pangea rifting—Newark Basin, USA. *Geochemistry* **2022**, *82*, 125918. [\[CrossRef\]](#)
72. Steckler, M.S.; Omar, G.I.; Karner, G.D.; Kohn, B.P. Pattern of hydrothermal circulation within the Newark basin from fission-track analysis. *Geology* **1993**, *21*, 735–738. [\[CrossRef\]](#)
73. Jones, B.; Renaut, R.W. Microstructural changes accompanying the opal-A to opal-CT transition: New evidence from the siliceous sinters of Geysir, Haukadalur, Iceland. *Sedimentology* **2007**, *54*, 921–948. [\[CrossRef\]](#)
74. Lynne, B.Y.; Campbell, K.A.; James, B.J.; Browne, P.R.L.; Moore, J. Tracking crystallinity in siliceous hot-spring deposits. *Am. J. Sci.* **2007**, *307*, 612–641. [\[CrossRef\]](#)
75. Heaney, P.J. A proposed mechanism for the growth of chalcedony. *Contrib. Mineral. Petrol.* **1993**, *115*, 66–74. [\[CrossRef\]](#)

76. Hartmann, L.A.; Antunes, L.M.; Rosenstengel, L.M. Stratigraphy of amethyst geode-bearing lavas and fault-block structures of the Entre Rios mining district, Paraná volcanic province, southern Brazil. *Ann. Braz. Acad. Sci.* **2014**, *86*, 187–198. [\[CrossRef\]](#)
77. Baggio, S.B.; Hartmann, L.A.; Andrade, R.H.P.; Rizzotto, G.J.; Duarte, S.K.; Knijnik, D.B.; Simões-Neto, J.A. Basalt stratigraphy and silica gossans in Campo Grande and Serra de Maracaju, Mato Grosso do Sul, Paraná Volcanic Province. *Ore Geol. Rev.* **2015**, *69*, 73–87. [\[CrossRef\]](#)
78. Li, B.; Kong, Q.; Wang, G.; Liu, F.; Guo, L.; Liu, C.; Liao, F.; Shi, Z. Controls on the behaviors of rare earth elements in acidic and alkaline thermal springs. *Appl. Geochem.* **2022**, *143*, 105379. [\[CrossRef\]](#)
79. Gislason, S.R.; Oelkers, E.H. Mechanism, rates, and consequences of basaltic glass dissolution: II. An experimental study of the dissolution rates of basaltic glass as a function of pH and temperature. *Geochim. Cosmochim. Acta* **2003**, *67*, 3817–3832. [\[CrossRef\]](#)
80. Gilg, H.A.; Morteau, G.; Kostitsyn, Y.; Preinfalk, C.; Gatter, I.; Streider, A.J. Genesis of amethyst geodes in basaltic rocks of the Serra Geral Formation (Ametista do Sul, Rio Grande do Sul, Brazil): A fluid inclusion, REE, oxygen, carbon, and Sr isotope study on basalt, quartz, and calcite. *Miner. Depos.* **2003**, *38*, 1009–1025. [\[CrossRef\]](#)
81. Commin-Fischer, A.; Berger, G.; Polyé, M.; Dubois, M.; Sardini, P.; Beaufort, D.; Formoso, M. Petrography and chemistry of SiO₂ filling phases in the amethyst geodes from the Serra Geral Formation deposit, Rio Grande do Sul, Brazil. *J. South Am. Earth Sci.* **2010**, *29*, 751–760. [\[CrossRef\]](#)
82. Götze, J.; Stanek, K.; Orozco, G.; Liesegang, M.; Mohr-Westheide, T. Occurrence and distribution of moganite and opal-CT in agates from Paleocene/Eocene tuffs, El Picado (Cuba). *Minerals* **2021**, *11*, 531. [\[CrossRef\]](#)
83. Franzson, H.; Zierenberg, R.; Schiffman, P. Chemical transport in geothermal systems in Iceland: Evidence from hydrothermal alteration. *J. Volcanol. Geotherm. Res.* **2008**, *173*, 217–229. [\[CrossRef\]](#)
84. Jeong, G.Y.; Sohn, Y.K. Mineralogy and microtextures of basaltic glass alteration in hyaloclasite, Jeju Island, Korea. *J. Anal. Sci. Technol.* **2011**, *2*, 13–22. [\[CrossRef\]](#)
85. Ducasse, T.; Gourgiotis, A.; Pringle, E.; Moynier, F.; Frugier, P.; Jollivet, P.; Gin, S. Alteration of basaltic glass in silica saturated conditions: Analogy with nuclear glass. *Appl. Geochem.* **2018**, *97*, 19–31. [\[CrossRef\]](#)
86. Prause, S.; Weisenberger, T.B.; Kleine, B.I.; Monien, P.; Rispoli, C.; Stefánsson, A. Alteration of basaltic glass within the Surtsey hydrothermal system, Iceland—Implication to oceanic crust seawater interaction. *J. Volcanol. Geotherm. Res.* **2022**, *429*, 107581. [\[CrossRef\]](#)
87. Pratt, L.M.; Shaw, C.A.; Burruss, R.C. Thermal histories of the Hartford and Newark basins inferred from maturation indices of organic matter. In *Studies of the Early Mesozoic Basins of the Eastern United States*; Froelich, A.J., Robinson, G.R., Jr., Eds.; Bulletin 1776; U.S. Geological Survey: Reston, VA, USA, 1988; pp. 58–63.
88. Clayton, R.N.; O’Neil, J.R.; Mayeda, T.K. Oxygen isotope exchange between quartz and water. *J. Geophys. Res.* **1972**, *77*, 3057–3067. [\[CrossRef\]](#)
89. Kent, D.V.; Tauxe, L. Corrected Late Triassic latitudes for continents adjacent to the North Atlantic. *Science* **2005**, *307*, 240–244. [\[CrossRef\]](#)
90. Fricke, H.C.; O’Neil, J.R. The correlation between ¹⁸O/¹⁶O ratios of meteoric water and surface temperature: Its use in investigating terrestrial climate change over geologic time. *Earth Planet. Sci. Lett.* **1999**, *170*, 181–196. [\[CrossRef\]](#)
91. Michard, A. Rare earth element systematics in hydrothermal fluids. *Geochim. Cosmochim. Acta* **1989**, *53*, 745–750. [\[CrossRef\]](#)
92. Bau, M. Scavenging of dissolved yttrium and rare earths by precipitating iron oxyhydroxide: Experimental evidence for Ce oxidation, Y-Ho fractionation, and lanthanide tetrad effect. *Geochim. Cosmochim. Acta* **1999**, *63*, 67–77. [\[CrossRef\]](#)
93. Liu, H.; Pourret, O.; Guo, H.; Bonhoure, J. Rare earth elements sorption to iron oxyhydroxide: Model development and application to groundwater. *Appl. Geochem.* **2017**, *87*, 158–166. [\[CrossRef\]](#)
94. Munemoto, T.; Ohmori, K.; Iwatsuki, T. Rare earth elements (REE) in deep groundwater from granite and fracture-filling calcite in the Tono area, central Japan: Prediction of REE fractionation in paleo- to present-day groundwater. *Chem. Geol.* **2015**, *417*, 58–67. [\[CrossRef\]](#)
95. Pan, Y.; Li, D.; Feng, R.; Wiens, E.; Chen, N.; Chernikov, R.; Götze, J.; Lin, J. Uranyl binding mechanism in microcrystalline silicas: A potential missing link for uranium mineralization by direct uranyl co-precipitation and environmental implications. *Geochim. Cosmochim. Acta* **2021**, *292*, 518–531. [\[CrossRef\]](#)
96. Smedley, P.L.; Kinniburgh, D.G. Uranium in natural waters and the environment: Distribution, speciation and impact. *Appl. Geochem.* **2023**, *148*, 105534. [\[CrossRef\]](#)
97. Möller, P.; Dulski, P.; De Lucia, M. REY patterns and their natural anomalies in waters and brines: The correlation of Gd and Y anomalies. *Hydrology* **2021**, *8*, 116. [\[CrossRef\]](#)

Disclaimer/Publisher’s Note: The statements, opinions and data contained in all publications are solely those of the individual author(s) and contributor(s) and not of MDPI and/or the editor(s). MDPI and/or the editor(s) disclaim responsibility for any injury to people or property resulting from any ideas, methods, instructions or products referred to in the content.